BETA - GAMMA - GAMMA CORRELATION IN Mn^{56}: A TEST OF TIME REVERSAL INVARIANCE

by

Martin Henry Garrell
B.A., Princeton University, 1960
M.S., University of Illinois, 1963

Ph.D. Dissertation
June, 1966

BETA-GAMMA-GAMMA CORRELATION IN Mn^{56}

A TEST OF TIME REVERSAL INVARIANCE

Martin Henry Garrell, Ph.D.

Department of Physics

University of Illinois, 1966

An experiment to measure time reversal violation in two β-γ-γ cascades of Mn^{56} (2.58 h) is discussed. We show how one measures the interference terms in β-γ-γ correlations using experimental quantities. We explain in detail the systematic errors involved in an accurate correlation experiment and point out the inherent limitations of such an experiment for time reversal measurements. Particular attention is given to descriptions of the electronics system used. From measurements of the interference terms in two γ transitions of Mn^{56}, we conclude that the phase difference between M1 and E2 reduced matrix elements is $(3.3 \pm 3.0) \cdot 10^{-2}$ and $(-4.3 \pm 4.0) \cdot 10^{-2}$ for the 1.81 and 2.12 MeV transitions respectively.

ACKNOWLEDGEMENTS

The author wishes to express sincere appreciation to the following people who aided him in this experiment:

Professor Hans Frauenfelder, who provided ideas, impetus, and understanding of many of the basic problems. With him, the many years of graduate study have been often hectic, but always thoroughly enjoyable and educational.

Professor David Sutton, without whose knowledge of electronics and insight into experimental physics, the experiment could not have been performed.

Mr. Daniel Ganek, whose help in setting up the electronics, preparing sources, and programming data was invaluable.

The staff of the University of Illinois Reactor Laboratory, especially Messrs. Gerald Beck, Paul Hesselman, and Sidney Boudreaux, who put in long hours and weeks irradiating our samples.

The staff of the Physics Research Laboratory, who made available the facilities and apparatus needed for the experiment.

Mrs. Barbara Anderson, who typed this thesis.

The author also wishes to thank many others who helped him in his academic career, including Professors Peter Debrunner, Giovanni DePasquali, Hendrik de Waard, and Gerald Almy, Mr. Muzaffer Atac, and Drs. Rollin Morrison and David Hafemeister.

The author wishes to express his appreciation to his wife Janet, whose understanding and encouragement were vital to him in the sometimes discouraging years of research and graduate study.

Finally, the author acknowledges the inspiration given to him by the fields and streams of the Midwest.

TABLE OF CONTENTS

I. INTRODUCTION

In 1957, when parity (P) and charge conjugation (C) violation were found for weak interactions, physicists began to ask whether time reversal (T) invariance existed for every physical process. At that time and for seven years afterwards, all experiments indicated T invariance.* Because all present field theories are invariant with respect to the product of C, P, and T taken in any order, T invariance implies invariance of the combined operation CP.

Then, in 1964, Christenson, Cronin, Fitch, and Turlay [1] discovered the two-pion-decay mode of the long-lived component K_2^0 of the neutral K meson. Since the two-pion-decay mode is of different CP than the predominant three-pion mode, the K_2^0 decay violates CP invariance. Because of the CPT theorem, CP breakdown implies T violation. Many suggestions were offered as explanations for the violation of CP and T. The hypothesis of Bernstein, Feinberg, and Lee [2] that T violation could arise in the electromagnetic interaction is of particular interest to us for our experiment.

From the work of Lloyd [3] one can show that T invariance has the following consequence: The ratio of certain reduced matrix elements which occur in the theory of angular correlations is real. Thus, one possible way to test for T violation is to look at the interference term in a mixed γ transition and to try to detect the imaginary part of the reduced matrix element ratio. Because this interference term is small, it is difficult to measure.

---

*For discussions of the symmetry principles, see J. J. Sakurai, Invariance Principles and Elementary Particles, (Princeton University Press, Princeton, 1964) and T. D. Lee, Phys. Today 19, #3, 23 (1966).

My thesis is based on a suggestion of Lee and Yang[4] -- amplified by Henley and Jacobsohn[5], Stichel[6], and DeSabbata[7] -- that T invariance can be tested in nuclear interactions by means of β-γ-γ angular correlation experiments. Fuschini, Gadjokov, Maroni, and Veronesi[8] performed experiments of this type in 1963-1964 with Ca^{47} and Rh^{106}. In the latter case, they claimed to have measured an interference term $\tilde{\epsilon} = (5 \pm 7) \cdot 10^{-4}$ from which they found the phase angle of the reduced matrix element ratio $\eta \approx \sin \eta = (3 \pm 4) \cdot 10^{-2}$.

We have tested time reversal invariance using two triple cascades in Mn^{56} (2.58 h). In each cascade a Gamow-Teller decay is followed by an electromagnetic M1-E2 mixed transition and then by a pure E2 transition. We chose Mn^{56} for our experiment for two reasons. The two cascades have mixing ratios that are different in sign and magnitude, and γ's of interest are easily resolved by scintillation detectors.

Our experiment differs from its predecessors in several respects. We used an elaborate system of modular electronics in order to obtain overall stability, high coincidence counting efficiency, and accurate accidental count rate corrections. We arranged our counters and interpreted our data in such a way as to reduce systematic errors. Finally, we were able to obtain smaller statistical errors in the measurement of the interference term. For the two cascades observed, we found the results given in Table 1.

The second chapter of this thesis is devoted to a brief discussion of the decay of Mn^{56}. The following chapter deals with the triple correlation equation and its application to our experiment. The physical configurations of the experiment (sources, counters, etc.), the conditions for running the experiment, and the essentials of the electronics circuitry are described in Chapter IV. The final chapter presents the data that

Table 1

Experimental Results for $\tilde{\epsilon}$, $(\delta\eta)$, and η

E_γ	1.81 MeV	2.12 MeV
δ	0.18	-0.28
$\tilde{\epsilon}$	$(3.1 \pm 2.9) \cdot 10^{-4}$	$(6.5 \pm 6.0) \cdot 10^{-4}$
$(\delta\eta)$	$(5.9 \pm 5.5) \cdot 10^{-3}$	$(12.2 \pm 11.2) \cdot 10^{-3}$
η	$(3.3 \pm 3.0) \cdot 10^{-2}$	$(-4.3 \pm 4.0) \cdot 10^{-2}$

were accumulated and an interpretation of these data.

Three appendices follow. The first is a summary of DeSabbata's[7] method for analyzing the $\beta-\gamma-\gamma$ correlation as it applies to the Mn^{56} cascades, the second is a detailed discussion of the electronics, and the last presents an example of data analysis for a typical run.

II. DECAY OF Mn^{56}

A. The Cascade

The decay of Mn^{56}, as illustrated in Figure 1, has two branches that follow the $3^+ \longrightarrow 2^+ \longrightarrow 2^+ \longrightarrow 0^+$ spin sequence. I shall refer to these branches in all that follows as the 1.81 MeV or 24% branch and the 2.12 MeV or 15% branch, according to the energies of the first (mixed)gammas of the cascades or according to the branching ratios.

B. The Reduced Matrix Element Ratios

The reduced matrix element ratio for a mixed gamma transition enters into the $\beta\gamma\gamma$ correlation equations, as shown in Appendix A. Its role in the determination of the time reversal violation is discussed in the following chapter. Several authors have measured the reduced matrix element ratios for both mixed gammas. [9,10,11] Averaging their experimental values, one obtains $= +0.18 \pm 0.03$ for the 1.81 MeV transition and -0.28 ± 0.03 for the 2.12 MeV transition. As a check on our coincidence circuitry, we also measured these reduced matrix element ratios by means of standard correlation techniques. We found values of 0.13 ± 0.03 and -0.24 ± 0.02, in reasonable agreement with the above.

Having two cascades of about equal energy but with different δ's is advantageous for our experiment. By a suitable choice of energy discriminator levels, we can observe triple correlations for both cascades in the same experiment. We expect to get two independent determinations of time reversal violation in this manner.

Figure 1. Decay scheme of Mn^{56}. Only predominant branches are shown.

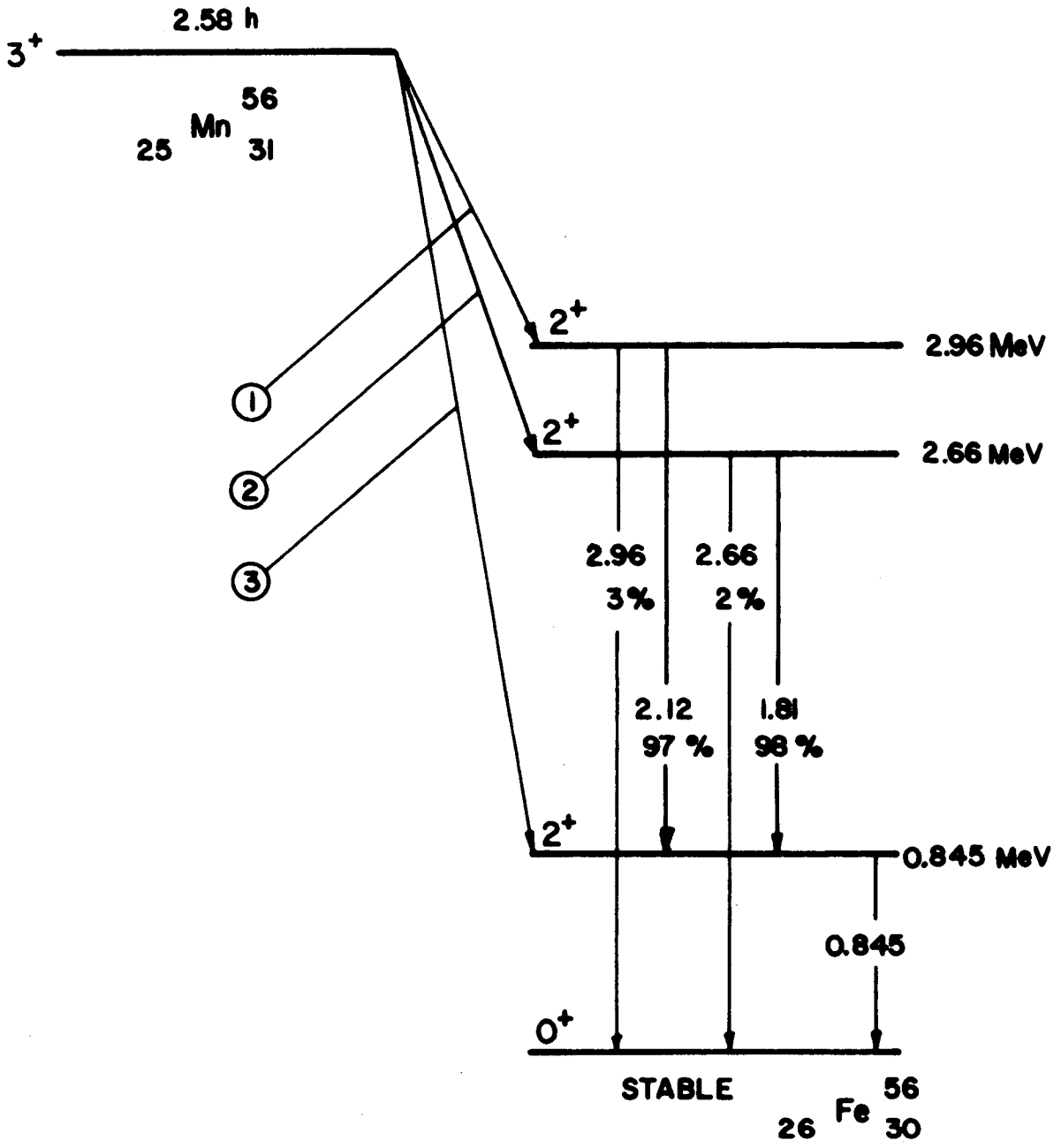

β BRANCH	MAXIMUM ENERGY (MeV)	BRANCHING RATIO	f t VALUE
①	0.750	15 %	5.4
②	1.05	24 %	5.7
③	2.86	60 %	7.0

C. Scintillation Spectra

The typical gamma and beta spectra of Mn^{56} which are shown in Figures 2a and 2b were obtained with our scintillation detectors (described in Chapter IV). The shaded portions of the spectra show the energies of interest for the coincidence experiment.

Figure 2a. Typical gamma spectrum of Mn^{56} source. The shaded portions are regions used for the coincidence experiment. The lower shaded portion is the 0.845 MeV window, and the upper shaded portion is used for display and storage in the multichannel analyzer.

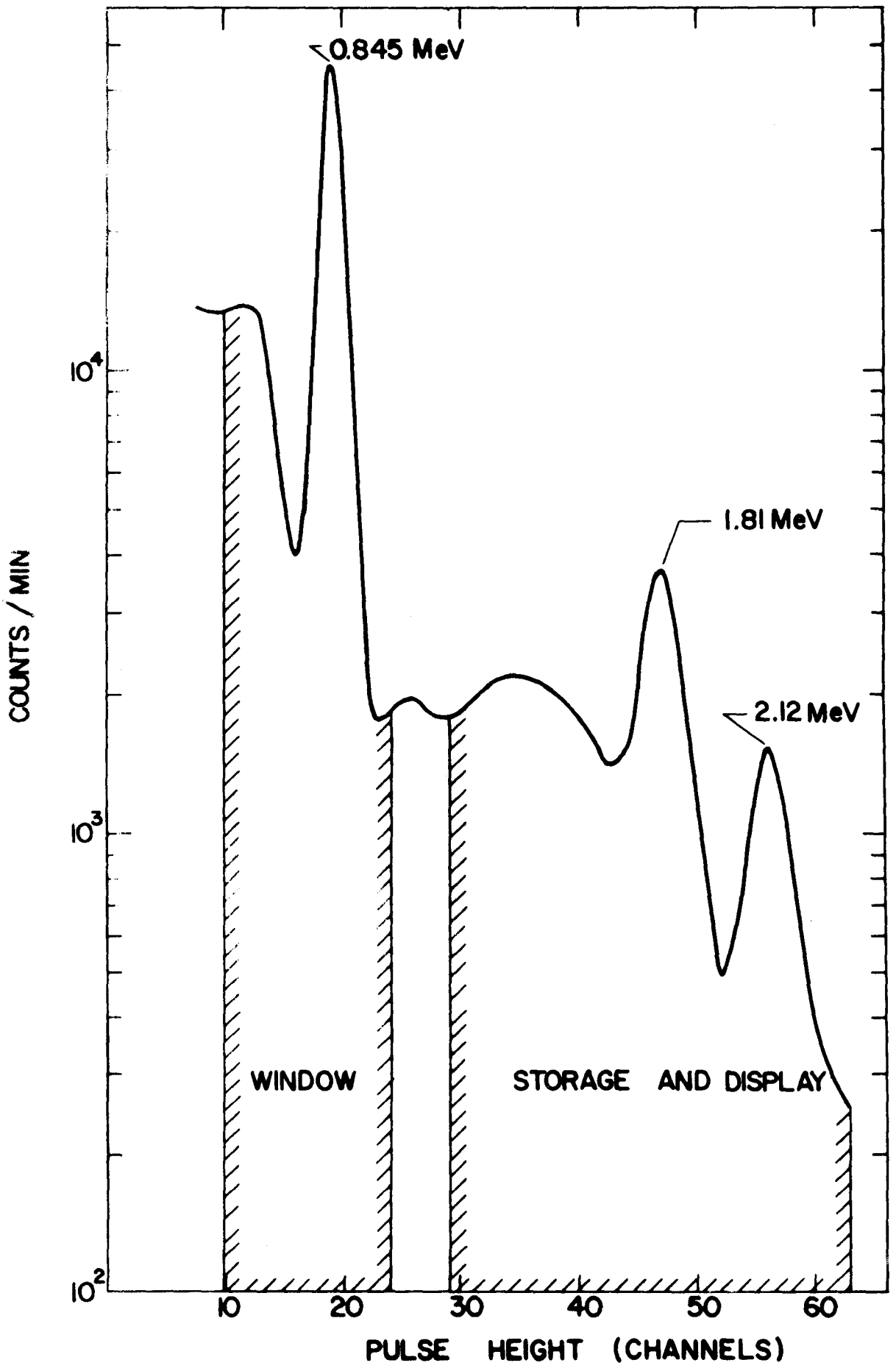
0.845 MeV
1.81 MeV
2.12 MeV
10^4
10^3
10^2
COUNTS / MIN
WINDOW
STORAGE AND DISPLAY
10
20
30
40
50
60
PULSE HEIGHT (CHANNELS)

Figure 2b. Typical beta spectrum of Mn^{56}. Shaded portion is used for $\beta\gamma\gamma$ coincidences.

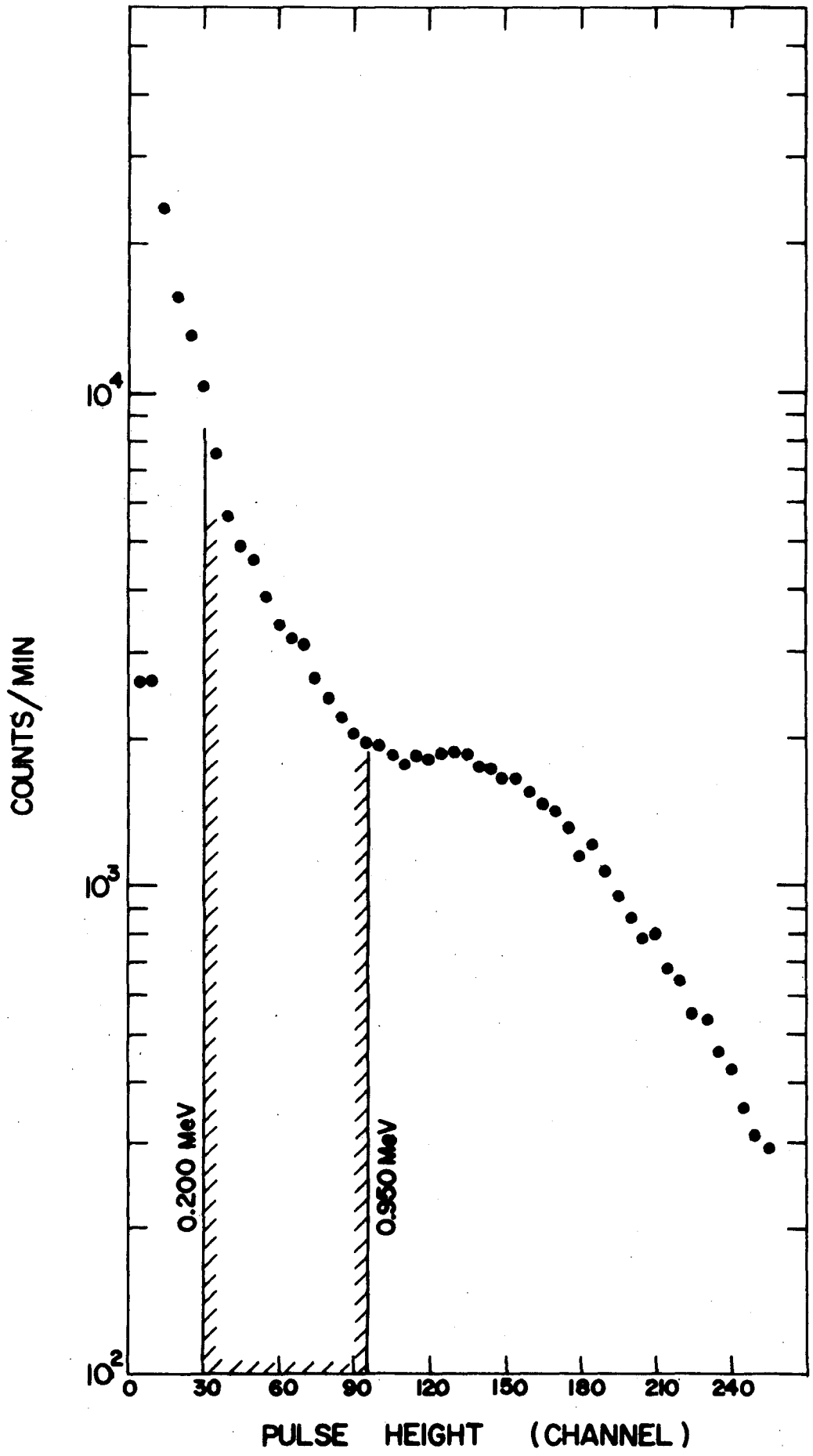
COUNTS/MIN
10^4
10^3
10^2
0.200 MeV
0.950 MeV
0
30
60
90
120
150
180
210
240
PULSE HEIGHT (CHANNEL)

III. THEORY

Having introduced the cascade of Mn^{56} and discussed the branches of interest in Chapter II, we now use the angular correlation results of Appendix A. According to these results, the normalized probability of a beta and subsequent gammas emerging in various directions (in a $3^+ \rightarrow 2^+ \rightarrow 2^+ \rightarrow 0^+$ cascade) is

$$W_{\beta\gamma\gamma} = 1 + A_{22} P_2(\hat{k}_{\gamma_1} \cdot \hat{k}_{\gamma_2}) + A_{44} P_4(\hat{k}_{\gamma_1} \cdot \hat{k}_{\gamma_2}) + \epsilon(\hat{k}_{\gamma_1}, \hat{k}_{\gamma_2}, \hat{k}_\beta) \qquad (1)$$

where

$$A_{22} = \left(0.250 + 0.732\left(\frac{\delta^* + \delta}{2}\right) - 0.077\,|\delta|^2\right)/(1 + |\delta|^2)$$

$$A_{44} = 0.327\,|\delta|^2/(1 + |\delta|^2)$$

$$\delta = \langle E2\rangle / \langle M1\rangle$$

$$\epsilon = 0.245\,\lambda\, v_\beta/c\,(\delta\eta)/(1 + |\delta|^2)$$

$$\lambda = (\hat{k}_{\gamma_1} \cdot \hat{k}_{\gamma_2})\,(\hat{k}_\beta \cdot (\hat{k}_{\gamma_1} \times \hat{k}_{\gamma_2}))$$

$$(\delta\eta) = \frac{i(\delta - \delta^*)}{2} = \frac{i}{2}\,\frac{(\langle M1\rangle^* \langle E2\rangle - \langle M1\rangle \langle E2\rangle^*)}{\langle M1\rangle \langle M1\rangle^*} \quad .$$

Note that $\int_{\text{all dirns.}} W_{\beta\gamma\gamma} = 1$. The $\hat{k}$'s are unit vectors in the directions of the outgoing particles, and v_β/c is the velocity of the β.

A. Inspection of ϵ

From the work of Lloyd,[3] one can show that the reduced matrix element ratio δ is complex if and only if the current between nucleons contains odd and even parts under time reversal. If this current is not mixed, δ will be real and $(\delta\eta) = 0$. Hence, detection of non-vanishing ϵ is tantamount to detection of time reversal violation.

We can now interpret $(\delta\eta)$ in terms of real and imaginary parts of complex reduced matrix elements. If we let $\langle M1\rangle = M + im$ and $\langle E2\rangle = E + ie$, where $M \gg m$ and $E \gg e$, then

$$(\delta\eta) \cong \frac{E}{M}\left(\frac{m}{M} - \frac{e}{E}\right) . \qquad (2)$$

This is seen to be consistent with $(\delta\eta) = \frac{i}{2}(\delta - \delta^*)$ if we take

$$\delta = \frac{E+ie}{M+im} \cong \frac{E}{M}\left(1 + i\left(\frac{e}{E} - \frac{m}{M}\right)\right) . \qquad (3)$$

$(\delta\eta)$ can be written

$$(\delta\eta) = -\,\mathrm{Im}(\delta) \cong \bar{\delta}(\eta_{M1} - \eta_{M2}) \qquad (4)$$

where

$$\bar{\delta} = E/M$$
$$\eta_{M1} = m/M$$
$$\eta_{E2} = e/E$$

Because the quantity $\bar{\delta}$ corresponds in first order to the experimental reduced matrix element ratio which has been accurately determined for both 1.81 MeV and 2.12 MeV transitions from $\gamma\gamma$ correlations, and because λ and v_β/c can also be calculated for our experiment, we can therefore measure the phase difference $\eta = (\eta_{M1} - \eta_{E2}) = \frac{m}{M} - \frac{e}{E}$. If the hypothesis of Bernstein, Feinberg and Lee [2] is correct, we should expect the ratios e/E and m/M to be $O(\alpha/2\pi)$, since these quantities are proportional to the ratios of even currents to odd currents.*

---

*In accord with a recent paper by Henley and Jacobsohn,[13] we have assumed in all the above discussion that, although a breakdown of the Born approximation may also be responsible for nonvanishing $(\delta\eta)$, the effect of this breakdown will be several orders of magnitude smaller than the effect of time reversal-violating nuclear currents.

B. Experimental Measurement of Triple Correlations.

In an experiment in which we are counting true triple coincidences using three arbitrary counters and two two-fold coincidence circuits, the number of true triple coincidences per second is

$$\eta_{123} = N_0 P_1 P_{1\text{-}2} P_{12\text{-}3} F_1 \varepsilon_1 \Omega_1 F_2 \varepsilon_2 \Omega_2 F_3 \varepsilon_3 \Omega_3 \varepsilon_{12} \varepsilon_{(12)3} W_{123}(\hat{k}_1, \hat{k}_2, \hat{k}_3) \qquad (5)$$

where

N_0 = number of disintegrations per second.

P_1 = probability of emission of particle 1.

$P_{1\text{-}2}$ = probability for emission of particle 2 if particle 1 has been emitted.

$P_{12\text{-}3}$ = probability for emission of particle 3 if particles 1 and 2 have been emitted.

F_i = relative width of energy selection for i^{th} particle.

ε_i = efficiency of i^{th} counter for detecting i^{th} particle.

Ω_i = solid angle subtended by i^{th} detector at the source.

ε_{12} = coincidence efficiency of the first two-fold circuit that fires on each coincidence between particles 1 and 2.

$\varepsilon_{(12)3}$ = coincidence efficiency of the second two-fold circuit that fires whenever the output of the first circuit is in coincidence with a pulse due to particle 3.

W_{123} = probability for detecting triple coincidences as a function of particle directions, defined such that: $\int_{\text{all dirns.}} W_{123} = 1$.

In the arrangement that we used (detectors are shown in Figure 3) four possible types of triple coincidences can be detected. These possibilities are illustrated in Figure 4.

Figure 3. Arrangement of detectors for triple correlation experiment and possible triple coincidence event.

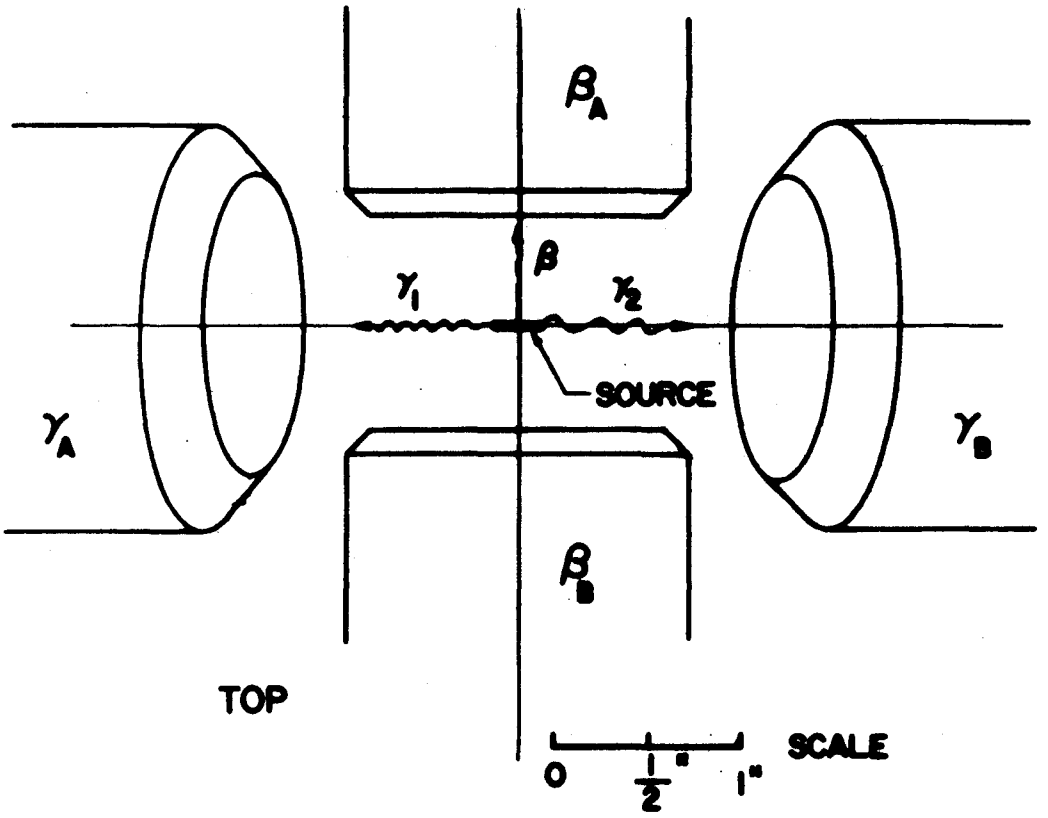
β_A
β
γ_1
γ_2
SOURCE
γ_A
γ_B
β_B
TOP
SCALE
0
$\frac{1}{2}$"
1"

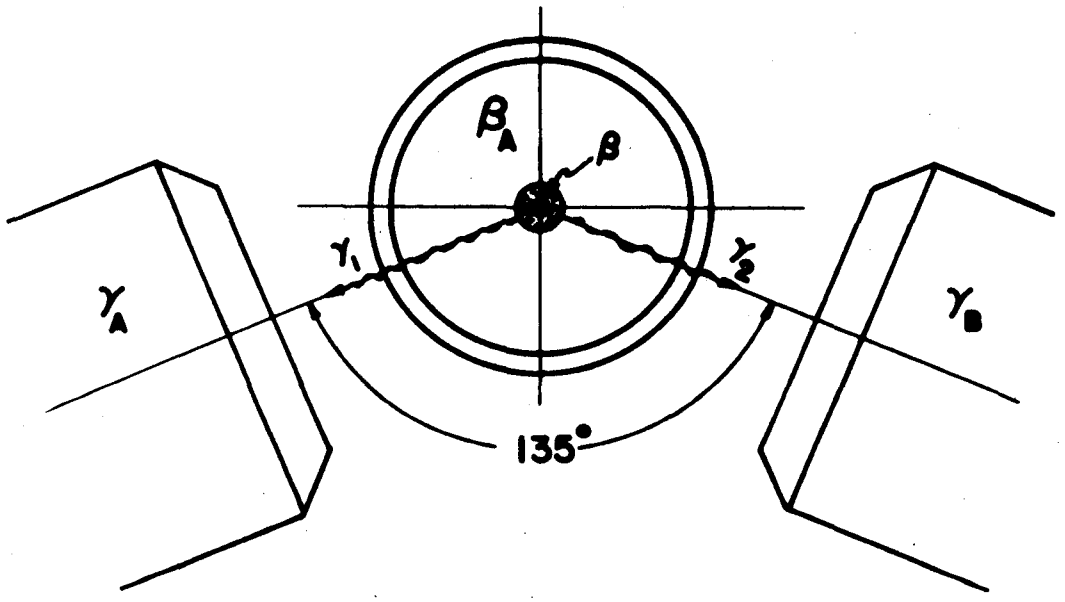
β_A
β
γ_1
γ_2
γ_A
γ_B
135°
FRONT

Figure 4. Four possible triple coincidence events for detection as seen in top view of Figure 3. $\lambda = \hat{k}_\beta \cdot (\hat{k}_{\gamma_1} \times \hat{k}_{\gamma_2}) \cdot (\hat{k}_{\gamma_1} \cdot k_{\gamma_2})$

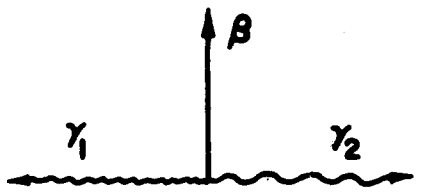

(1) $\lambda = +1/2$

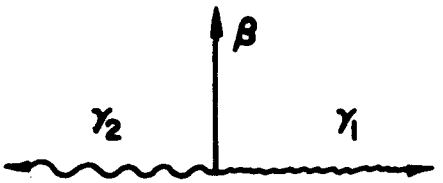

(2) $\lambda = -1/2$

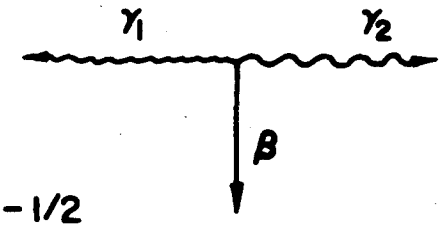

(3) $\lambda = -1/2$

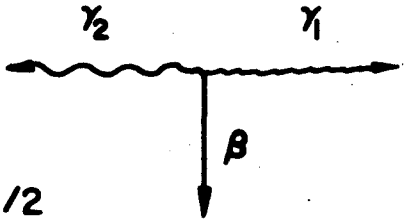

(4) $\lambda = +1/2$

TYPE 1 $$\eta_{\beta_A \gamma_{1A} \gamma_{2B}} = N_0 P_\beta P_{\beta-\gamma_1} P_{\beta\gamma_1-\gamma_2} F_{\beta_A} \varepsilon_{\beta_A} \Omega_{\beta_A} F_{\gamma_{1A}} \varepsilon_{\gamma_{1A}} \Omega_{\gamma_A} F_{\gamma_{2B}} \varepsilon_{\gamma_{2B}} \Omega_{\gamma_B} \times \varepsilon_{\gamma_{1A}\gamma_{2B}} \varepsilon_{(\gamma_{1A}\gamma_{2B})\beta_A} W^+ \quad (6)$$

TYPE 2 $$\eta_{\beta_A \gamma_{2A} \gamma_{1B}} = N_0 P_\beta P_{\beta-\gamma_1} P_{\beta\gamma_1-\gamma_2} F_{\beta_A} \varepsilon_{\beta_A} \Omega_{\beta_A} F_{\gamma_{2A}} \varepsilon_{\gamma_{2A}} \Omega_A F_{\gamma_{1B}} \varepsilon_{\gamma_{1B}} \Omega_{\gamma_B} \times \varepsilon_{\gamma_{2A}\gamma_{1B}} \varepsilon_{(\gamma_{2A}\gamma_{1B})\beta_A} W^-$$

TYPE 3 $$\eta_{\beta_B \gamma_{1A} \gamma_{2B}} = N_0 P_\beta P_{\beta-\gamma_1} P_{\beta\gamma_1-\gamma_2} F_{\beta_B} \varepsilon_{\beta_B} \Omega_{\beta_B} F_{\gamma_{1A}} \varepsilon_{\gamma_{1A}} \Omega_{\gamma_A} F_{\gamma_{2B}} \varepsilon_{\gamma_{2B}} \Omega_{\gamma_B} \times \varepsilon_{\gamma_{1A}\gamma_{2B}} \varepsilon_{(\gamma_{1A}\gamma_{2B})\beta_B} W^-$$

TYPE 4 $$\eta_{\beta_B \gamma_{2A} \gamma_{1B}} = N_0 P_\beta P_{\beta-\gamma_1} P_{\beta\gamma_1-\gamma_2} F_{\beta_B} \varepsilon_{\beta_B} \Omega_{\beta_B} F_{\gamma_{2A}} \varepsilon_{\gamma_{2A}} \Omega_{\gamma_A} F_{\gamma_{1B}} \varepsilon_{\gamma_{1B}} \Omega_{\gamma_B} \times \varepsilon_{\gamma_{1B}\gamma_{2A}} \varepsilon_{(\gamma_{1B}\gamma_{2A})\beta_B} W^+$$

W is the function (1), and we define W^+ and W^- according to the sign of λ . Then, in the experimental situation

$$W^{\pm} = 1 + A_{22} Q_{22} P_2(\hat{k}_{\gamma_1} \cdot \hat{k}_{\gamma_2}) + A_{44} Q_{44} P_4(\hat{k}_{\gamma_1} \cdot \hat{k}_{\gamma_2}) \pm \epsilon' \quad (7)$$

where $$\epsilon' = 0.245\ v\beta/c\ |\lambda|\ (\delta\eta)\ Q_1 Q_{22} / (1 + |\delta|^2) \quad . \quad (8)$$

$|\lambda| = 1/2$ for particles directed along the axes of Figure 3.

Q_1, Q_{22}, and Q_{44} are the geometrical attenuation coefficients due to the solid angles subtended by the counters at the source. If we measure the numbers of true coincidences of all four types during the same period of time and combine these numbers in the ratio

N_4 = (TYPE 1/TYPE 2) • (TYPE 4/TYPE 3)

$$= \left(\eta_{\beta_A \gamma_{1A} \gamma_{2B}} / \eta_{\beta_A \gamma_{1B} \gamma_{2A}}\right) \cdot \left(\eta_{\beta_B \gamma_{1B} \gamma_{2A}} / \eta_{\beta_B \gamma_{1A} \gamma_{2B}}\right)$$

$$= E_4 \left(1 + \tilde{\epsilon}\right)^2 / (1 - \tilde{\epsilon})^2$$

where

$$\tilde{\epsilon} = \frac{0.245\ v\beta/c\ \ |\lambda|\,(\delta\eta)\,Q_1\,Q_{22}\,/(1+|\delta|^2)}{1 + A_{22}\,Q_{22}\,P_2(3\pi/4) + A_{44}\,Q_{44}\,P_4(3\pi/4)} \qquad (9)$$

and

$$E_4 = \frac{\varepsilon_{(\gamma_{1A}\gamma_{2B})\beta_A}}{\varepsilon_{(\gamma_{2A}\gamma_{1B})\beta_A}} \cdot \frac{\varepsilon_{(\gamma_{2A}\gamma_{1B})\beta_B}}{\varepsilon_{(\gamma_{1A}\gamma_{2B})\beta_B}} \cong 1 \quad , \qquad (9')$$

we find

$$\tilde{\epsilon} \cong \tfrac{1}{2}(u-1)/(u+1) \qquad (10)$$

where $u = N_4/E_4$.

The uncertainty in $\tilde{\epsilon}$ is given by

$$\delta\tilde{\epsilon} \cong \left(1/N_{tot} + (\Delta/4)^2\right)^{1/2} . \qquad (11)$$

N_{tot} is the total number of true coincidence events, and Δ is the fluctuation in E_4 about unity. Δ arises because all four $(\gamma\gamma)\beta$ coincidences are not treated by identical electronics. When the systematic error $\Delta/4$ is much smaller than the statistical error $\sqrt{1/N_{tot}}$, then $\delta\tilde{\epsilon} \cong \sqrt{1/N_{tot}}$. Actual processing of experimental data involves accidental count rate corrections and background corrections. These increase the statistical error slightly. As $N_{tot} \to \infty$, $\delta\tilde{\epsilon} \to \Delta/4$. If all coincidence efficiencies were the same to within one part in 10^4, which is close to the practical limit for the experiment, we would expect $\Delta \simeq \sqrt{4 \cdot (10^{-8})}$ or $\Delta/4 \cong 5 \times 10^{-5}$.

C. Another Method for Determining $\tilde{\epsilon}$.

If we observe $\gamma\gamma$ coincidences at the same time that $\beta\gamma\gamma$ data are taken, there is another method of data processing. The number of true double coincidences per second in which γ_1 is counted by detector A and γ_2 is counted by detector B is

$$n_{\gamma_{1A}\gamma_{2B}} = N_0 P_{\gamma_1} P_{\gamma_1-\gamma_2} F_{\gamma_{1A}} \epsilon_{\gamma_{1A}} \Omega_{\gamma_A} F_{\gamma_{2B}} \epsilon_{\gamma_{2B}} \Omega_{\gamma_B} \epsilon_{\gamma_{1A}\gamma_{2B}} \times (1 + A_{22} Q_{22} P_2(\hat{k}_{\gamma_1} \cdot \hat{k}_{\gamma_2}) + A_{44} Q_{44} P_4(\hat{k}_{\gamma_1} \cdot \hat{k}_{\gamma_2})) . \quad (12)$$

The number of true double coincidences per second in which γ_2 is counted by detector A and γ_1 is counted by detector B is

$$n_{\gamma_{2A}\gamma_{1B}} = N_0 P_{\gamma_1} P_{\gamma_1-\gamma_2} F_{\gamma_{2A}} \epsilon_{\gamma_{2A}} \Omega_{\gamma_A} F_{\gamma_{1B}} \epsilon_{\gamma_{1B}} \Omega_{\gamma_B} \epsilon_{\gamma_{2A}\gamma_{1B}} \times (1 + A_{22} Q_{22} P_2(\hat{k}_{\gamma_1} \cdot \hat{k}_{\gamma_2}) + A_{44} Q_{44} P_4(\hat{k}_{\gamma_1} \cdot \hat{k}_{\gamma_2})) . \quad (12')$$

If we divide the number of triple coincidences of each type in (6) by the number of appropriate double coincidences in (12) and (12'), and then combine the data in the forms

$$N_A = \left(\text{TYPE 1} / N(\gamma_{1A}\gamma_{2B})\right) \cdot \left(N(\gamma_{2A}\gamma_{1B}) / \text{TYPE 2}\right) \; ; \; N_B = \left(\text{TYPE 4} / N(\gamma_{2A}\gamma_{1B})\right) \cdot \left(N(\gamma_A\gamma_{2B}) / \text{TYPE 3}\right) \quad (13)$$

where $N(y)$ = number of true events of type y,

we get

$$N_A = \left(W^+ / W^-\right) \cdot \frac{\epsilon_{(\gamma_{1A}\gamma_{2B})\beta_A}}{\epsilon_{(\gamma_{2A}\gamma_{1B})\beta_A}} \; ; \quad N_B = \left(\frac{W^+}{W^-}\right) \cdot \frac{\epsilon_{(\gamma_{2A}\gamma_{1B})\beta_B}}{\epsilon_{(\gamma_{1A}\gamma_{2B})\beta_B}} . \quad (14)$$

Then, using this method, we have two separate determinations of $\tilde{\epsilon}$, which was defined in (9).

$$\tilde{\epsilon}_A = (v_A - 1)/(v_A + 1) \; ; \quad \tilde{\epsilon}_B = (v_B - 1)/(v_B + 1) \quad (15)$$

Here

$$U_A = N_A/E_A \quad ; \quad U_B = N_B/E_B \qquad (16)$$

$$E_A = \frac{\varepsilon_{(\gamma_{1A}\gamma_{2B})\beta_A}}{\varepsilon_{(\gamma_{2A}\gamma_{1B})\beta_A}} \cong 1 \quad ; \quad E_B = \frac{\varepsilon_{(\gamma_{2A}\gamma_{1B})\beta_B}}{\varepsilon_{(\gamma_{1A}\gamma_{2B})\beta_B}} \cong 1$$

For this case, the uncertainty in $\tilde{\varepsilon}_A$ will be

$$\delta\tilde{\varepsilon}_A \cong \left(1/N_{totA} + \left(\frac{\Delta_A}{2}\right)^2 \right)^{1/2} . \qquad (17)$$

(Similarly for $\tilde{\varepsilon}_B$). N_{totA} is the total number of $\beta_A(\gamma\gamma)$ coincidence events, and Δ_A is the fluctuation of E_A about unity. If $\beta_A(\gamma\gamma)$ coincidence efficiencies were the same to within one part in 10^4, we might expect $\Delta_A = \sqrt{2 \cdot (10^{-8})}$ or $\frac{\Delta_A}{2} = 7.1 \times 10^{-5}$.

Because this method separates the analysis of $\beta_A(\gamma\gamma)$ and $\beta_B(\gamma\gamma)$ coincidences and because it brings in $\gamma\gamma$ coincidence data for normalization, it is not as symmetric as the method described in B, and additional errors may be introduced. For example, if the gamma detectors have different window settings $(F_{\gamma_{1A}} F_{\gamma_{2B}} \neq F_{\gamma_{2A}} F_{\gamma_{1B}})$ and a significant amount of $\gamma\gamma$ background (but not $\beta\gamma\gamma$ background) is present, $\tilde{\varepsilon}_A$ and $\tilde{\varepsilon}_B$ will be quite different unless we correct precisely for that background.

D. Statistics for Determination of $\tilde{\varepsilon}$, $(\delta\eta)$, and η.

Suppose we wish to determine $\tilde{\varepsilon}$ within a given standard deviation for either cascade of Mn^{56}. The numbers of true triple coincidences necessary are given in Tables 2a and 2b. Also included in these tables are values of $(\delta\eta)$ and η for each $\tilde{\varepsilon}$. In computing tables we have used attenuation coefficients for our experimental geometry -- $Q_{22} = 0.72$ and $Q_1 = 0.80$. The term $Q_{44}P_4A_{44}$ has been neglected since it is much smaller than $Q_{22}P_2A_{22}$. $\langle v/c \rangle$ for both branches was calculated by averaging over appropriate β spectra. $\langle v/c \rangle = 0.81$ for the 2.12 MeV branch and $\langle v/c \rangle = 0.83$ for the 1.81 MeV branch.

Table 2a

$\tilde{\epsilon}$, $(\delta\eta)$, η, and Statistics Needed for 24% Branch (1.81 MeV)

$\tilde{\epsilon}$	Statistics to Measure Std. Deviation of $\pm\tilde{\epsilon}$	$(\delta\eta) = 19.1 \times \tilde{\epsilon}$	$\eta = 5.55 \times (\delta\eta)$
10^{-2}	10^{4}	19.1×10^{-2}	1.06
5×10^{-3}	4×10^{4}	9.55×10^{-2}	5.30×10^{-1}
10^{-3}	10^{6}	19.1×10^{-3}	1.06×10^{-1}
5×10^{-4}	4×10^{6}	9.55×10^{-3}	5.30×10^{-2}
10^{-4}	10^{8}	1.91×10^{-3}	1.06×10^{-2}
10^{-5}	10^{10}	1.91×10^{-4}	1.06×10^{-3}

Table 2b

$\tilde{\epsilon}$, $(\delta\eta)$, η , and Statistics Needed for 15% Branch (2.12 MeV)

$\tilde{\epsilon}$	Statistics to Measure Std. Deviation of $\pm\tilde{\epsilon}$	$(\delta\eta) = 18.7 \times \tilde{\epsilon}$	$\eta = -3.57 \times (\delta\eta)$
10^{-2}	10^{4}	18.7×10^{-2}	-6.67×10^{-1}
5×10^{-3}	4×10^{4}	9.35×10^{-2}	-3.34×10^{-1}
10^{-3}	10^{6}	1.87×10^{-2}	-6.67×10^{-2}
5×10^{-4}	4×10^{6}	9.35×10^{-3}	-3.34×10^{-2}
10^{-4}	10^{8}	1.87×10^{-3}	-6.67×10^{-3}
10^{-5}	10^{10}	1.87×10^{-4}	-6.67×10^{-4}

IV. EQUIPMENT AND PROCEDURES

In this chapter, we first describe the physical layout used for the experiment including detectors, sources, and source holders. The procedure is also discussed, and typical counting data are given. For coincidence measurements, we used a system of modular logic circuits. The essential aspects of the circuits are mentioned here, and a more detailed description follows in Appendix B.

A. Physical Layout

1. Detectors. The arrangement of our scintillation counters was shown in the last chapter (Figure 3). The gamma detectors were Harshaw 2" X 3" NaI(Tl) Xtals with 1/4" (45°) bevelled faces mounted on high quantum efficiency RCA 8575 photomultiplier tubes. To eliminate betas incident on these Xtals, 1/4" thick beryllium discs were mounted in front of them. The beta detectors were 1-3/4" X 1/4" discs of Pilot A plastic with 1/8" (45°) bevelled faces mounted on Philips 56AVP photomultiplier tubes. The plastic detectors were covered with two layers of quarter mil aluminum foil to exclude all light and were mounted on the phototubes by means of 1-3/4" X 1" lucite light pipes and Epox-E Pilot Bond. Each beta detector subtended a fractional solid angle of 0.200 ± 0.008, and each gamma detector subtended a fractional solid angle of 0.073 ± 0.001 at the center of the source.

2. Sources and Source Frame. The sources were metallic layers of manganese evaporated onto both sides of quarter mil mylar. Aluminum layers, approximately 0.006 mg/cm^2 served as bases for the manganese deposits. Several sources were prepared with manganese layers ranging from 0.05 to 0.12 mg/cm^2. Multiple scattering in the sources was negligible; the mean scattering angle of the lowest energy betas used in the

coincidence experiment was less than 12° .

The entire apparatus was mounted in an aluminum frame made of 1/16" and 1/32" sheet metal. The sources fitted into slotted lucite holders which slipped into the frame, and the counters were rigidly fixed to vee-shaped ways on the frame.

B. Procedure

Sources were inserted in the University of Illinois Triga Mark II reactor and exposed to a flux of about 1.8×10^{12} neutrons/cm^2, sec for periods ranging from twenty minutes to one hour. Within one hour after irradiation, the sources were placed in position, and coincidence data were taken for periods of three to eight hours. Typical counting data appear in Table 3. Originally, we intended to use more active sources, but we found that increased activity caused severe gain shifts and anode fatigue in the RCA 8575's.

C. Electronics

The basic block diagram of the electronics appears in Figure 5; to avoid confusion we show only one of the two $\beta(\gamma\gamma)$ coincidence circuits and only four of the six routing inputs to the multichannel analyzer. Details are explained in Appendix B. The main features are the following:

1. Accidental Count Rates. Accidental count rates were measured throughout the experiment. Rather than using separate coincidence circuitry for this purpose, we employed the same coincidence circuits that formed the true coincidences; this was done by using doubled pulses for certain events. Figures are included and details are explained in Appendix B.

Table 3

Typical Counting Data

Source #3
Irradiation Time: 30 min.
Run began 37 min. after irradiation
Time of run: 255 min.

Type of Event	Counts/sec at Beginning	Total Counts During Run	Counts/sec at End of Run
β_A singles window	1.57×10^5	1.29×10^9	4.32×10^4
β_B singles window	1.65×10^5	1.37×10^9	4.56×10^4
γ_B singles above 0.5 MeV	3.97×10^4	3.36×10^8	1.15×10^4
γ_A singles above 0.5 MeV	4.47×10^4	3.72×10^8	1.26×10^4
$\gamma\gamma$ coinc. (true + acc.)	5.56×10^2	4.56×10^6	1.53×10^2
$\beta_A(\gamma\gamma)$ coinc. (true + acc.)	6.95×10	5.70×10^5	1.92×10

Figure 5. Block diagram of logic circuitry and data storage.

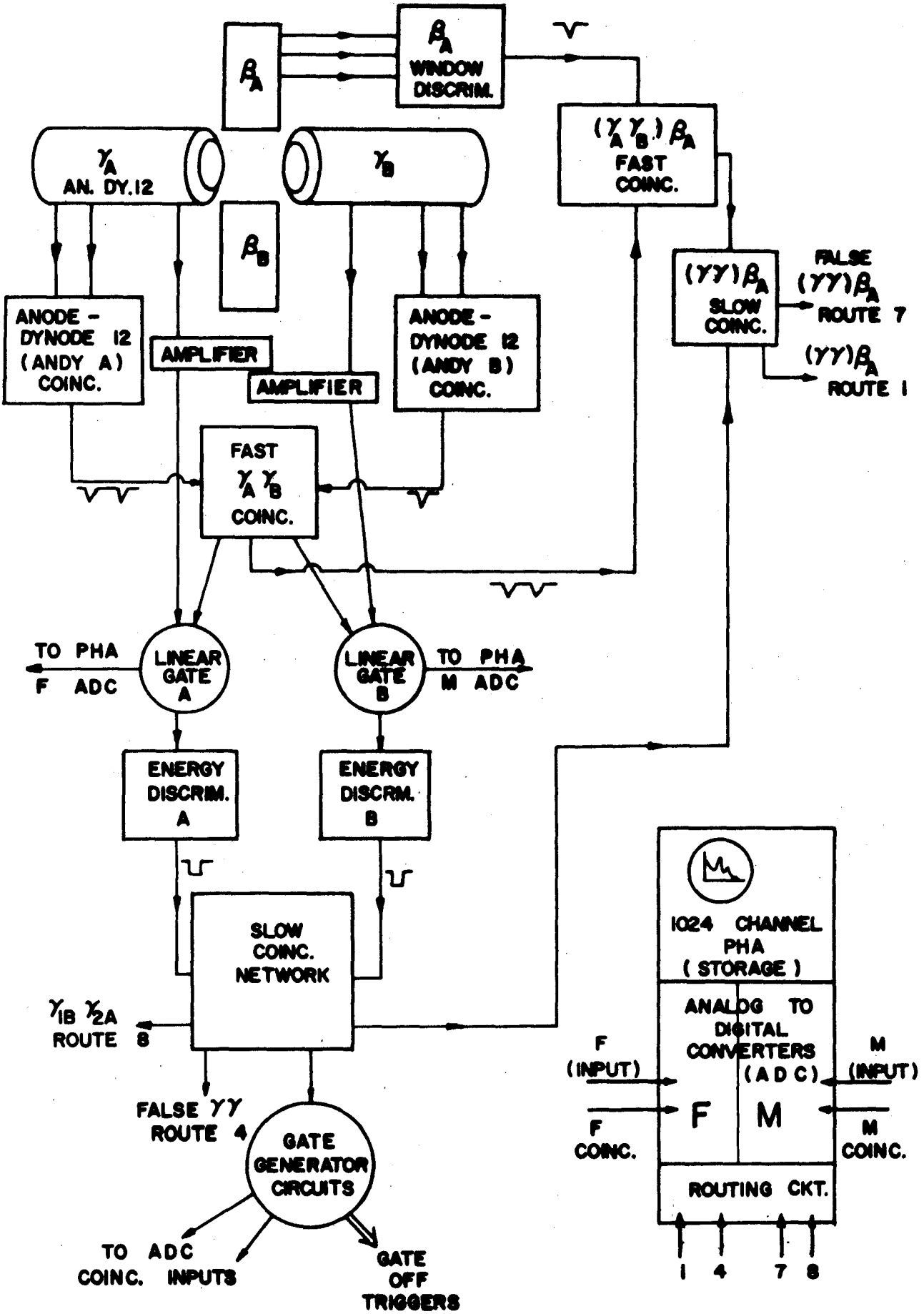
β_A
β_A WINDOW DISCRIM.
γ_A AN. DY. 12
γ_B
β_B
$(\gamma_A \gamma_B)\beta_A$ FAST COINC.
$(\gamma\gamma)\beta_A$ SLOW COINC.
FALSE $(\gamma\gamma)\beta_A$ ROUTE 7
$(\gamma\gamma)\beta_A$ ROUTE 1
ANODE - DYNODE 12 (ANDY A) COINC.
AMPLIFIER
AMPLIFIER
ANODE - DYNODE 12 (ANDY B) COINC.
FAST $\gamma_A \gamma_B$ COINC.
TO PHA F ADC
LINEAR GATE A
LINEAR GATE B
TO PHA M ADC
ENERGY DISCRIM. A
ENERGY DISCRIM. B
SLOW COINC. NETWORK
γ_{1B} γ_{2A} ROUTE 8
FALSE $\gamma\gamma$ ROUTE 4
GATE GENERATOR CIRCUITS
TO ADC COINC. INPUTS
GATE OFF TRIGGERS
1024 CHANNEL PHA (STORAGE)
ANALOG TO DIGITAL CONVERTERS (ADC)
F (INPUT)
M (INPUT)
F
M
F COINC.
M COINC.
ROUTING CKT.
1 4 7 8

2. Pulse Sampling. We sampled three pulses from each γ photomultiplier tube for use in both fast and slow coincidence circuits. Eighth dynode pulses from RCA 8575's were amplified by Stirrup double delay line amplifiers and passed into linear gates. Pulses were taken from the anodes and twelfth dynodes of the RCA 8575's, and coincidences were formed by the circuits denoted "AnDy". Fast rising anode pulses provided the timing, while dynode pulses set lower energy cutoffs of about 0.5 MeV for these AnDy circuits. AnDy pulses formed $\gamma\gamma$ fast coincidences which opened the linear gates for fifty nsec at the peaks of the amplified eighth dynode pulses.

3. Twofold Fast Coincidences. Twofold coincidences were used throughout the network. AnDy·AnDy or $\gamma\gamma$ fast coincidences mentioned in the preceding paragraph formed $\beta(\gamma\gamma)$ fast coincidences with β pulses from energy discriminators.

In Chapter III I pointed out the importance of having nearly-identical coincidence efficiencies (for the circuits that produce $\beta(\gamma\gamma)$ coincidences). We took delay curves and checked coincidence efficiencies several times during the data taking, and estimate that E_4 was within 2×10^{-4} of unity. From the delay curves, we estimate the resolving times to be 12 nsec and 17 nsec for the $\gamma\gamma$ and $\beta(\gamma\gamma)$ fast coincidence circuits, respectively. Our method of measuring coincidence efficiencies is discussed in Appendix B.

4. Pulse Height Analysis. We used a Nuclear Data 1024 channel pulse height analyzer for storage and display of coincidence information. We stored and displayed pulse height spectra of 1.81 MeV and 2.12 MeV coincidence γ's. To obtain a maximum amount of information, we stored some of the Compton spectra as well as the photopeaks, as Figure 2a. shows.

To eliminate dead time and pile-up problems, the analyzer was fed signals from the linear gates (These signals were stretched and amplified to suit the multichannel analyzer.) whenever the gates were opened by $\gamma\gamma$ coincidences. The energy discriminators and slow coincidence network differentiated between $\gamma_{1A}\gamma_{2B}$ and $\gamma_{2A}\gamma_{1B}$ coincidences. Both analog-to-digital converters of the analyzer were operated in coincidence modes with coincidence inputs provided by gate generators fed from the slow coincidence network. A selective storage or "routing" circuit in the analyzer sorted out different kinds of coincidences into sixteen groups of sixty-four channels. Routing input signals came from the slow coincidence circuits.

5. Trigger Gating. We used four gate generators to shut off many of the triggers in the system (i.e., triggers in the AnDy circuit, in the β discriminators, and in the γ energy discriminators) for several μsec whenever coincidence information was stored in the multichannel analyzer. This was done in order to avoid ambiguous routing.

6. Slow Coincidence Network. Slow coincidences were formed between 100 nsec and 50 nsec pulses produced by trigger circuits in the energy discriminators. Because the triggers in the energy discriminators were gated off after each coincidence pulse and because these triggers fired only when the linear gates were opened by coincidences, there were no accidental coincidences in the slow network.

7. Isolation. Four separate supplies provided power for the modular equipment. The triggers, AnDy circuits, etc. associated with each counter were powered by two different supplies, a third supply powered the $\gamma\gamma$ coincidence modules, and a fourth supply was used for the triggers and modules associated with $\beta(\gamma\gamma)$ coincidences. In this manner we avoided interaction between γ circuits and prevented the $\gamma\gamma$ coincidence circuits from knowing about β counting. The double delay line amplifiers were powered by a common supply, however.

V. DATA ANALYSIS AND RESULTS

Data were analyzed in three steps by a computer program. First, accidental counts were subtracted, next the 1.81 and 2.12 MeV photopeaks were separated, and finally $\tilde{\epsilon}$ and $\delta\tilde{\epsilon}_{st}$, the statistical error in $\tilde{\epsilon}$, were calculated for each transition. Results of the analysis, considerations given to errors and background, etc. are discussed here. The analysis is explained in more detail in Appendix C.

A. Analysis

Using false coincidences as a measure of accidentals, we obtained numbers of true coincidences of four types ($\beta_A\gamma_{1A}\gamma_{2B}$, $\beta_A\gamma_{2A}\gamma_{1B}$, $\beta_B\gamma_{1A}\gamma_{2B}$, $\beta_B\gamma_{2A}\gamma_{1B}$) from the data stored in the multichannel analyzer. By comparing the Mn^{56} γ spectrum with superimposed γ spectra from Ce^{144} and Y^{88} (long lived isotopes with strong gamma transitions of 2.18 and 1.84 MeV respectively) we separated the two photopeaks of the Mn^{56} spectrum. $\tilde{\epsilon}$ was then calculated from equations (9) and (10) of Chapter II.

$$\tilde{\epsilon} = \frac{1}{2}\,(U-1)/(U+1) \qquad \text{where} \quad E_4 = 1 \qquad (18)$$

and $$U = \left(N(\beta_A\gamma_{1A}\gamma_{2B})/N(\beta_A\gamma_{2A}\gamma_{1B})\right)\cdot\left(N(\beta_B\gamma_{2A}\gamma_{1B})/N(\beta_B\gamma_{1A}\gamma_{2B})\right)$$

N(y) = number of true $\beta\gamma\gamma$ coincidences of type y (each photopeak taken separately)

Statistical errors in the $\tilde{\epsilon}$'s were calculated from statistical errors in the true coincidences. Results for the 1.81 and 2.12 MeV photopeaks are shown in the following figures and table. Figure 6 exhibits plots of $\tilde{\epsilon}$ and $\delta\tilde{\epsilon}_{st}$ for the first fifty runs. Table 4 gives cumulative results for 128 runs. In the table we also list values of $\chi^2(\tilde{\epsilon}_{Avg.})$ for all runs.

Table 4

Cumulative Results for First 128 Runs

E_γ	$\tilde{\epsilon}_{avg}$	$\delta\tilde{\epsilon}_{st}$	$\chi^2(\tilde{\epsilon}_{Avg.})$
1.81 MeV	3.11×10^{-4}	2.7×10^{-4}	141.6
2.12 MeV	6.51×10^{-4}	5.9×10^{-4}	147.3

Figure 6. Results of first fifty runs.

a. $\widetilde{\epsilon}$ versus run number for 1.81 MeV photopeak.

b. $\widetilde{\epsilon}$ versus run number for 2.12 MeV photopeak.

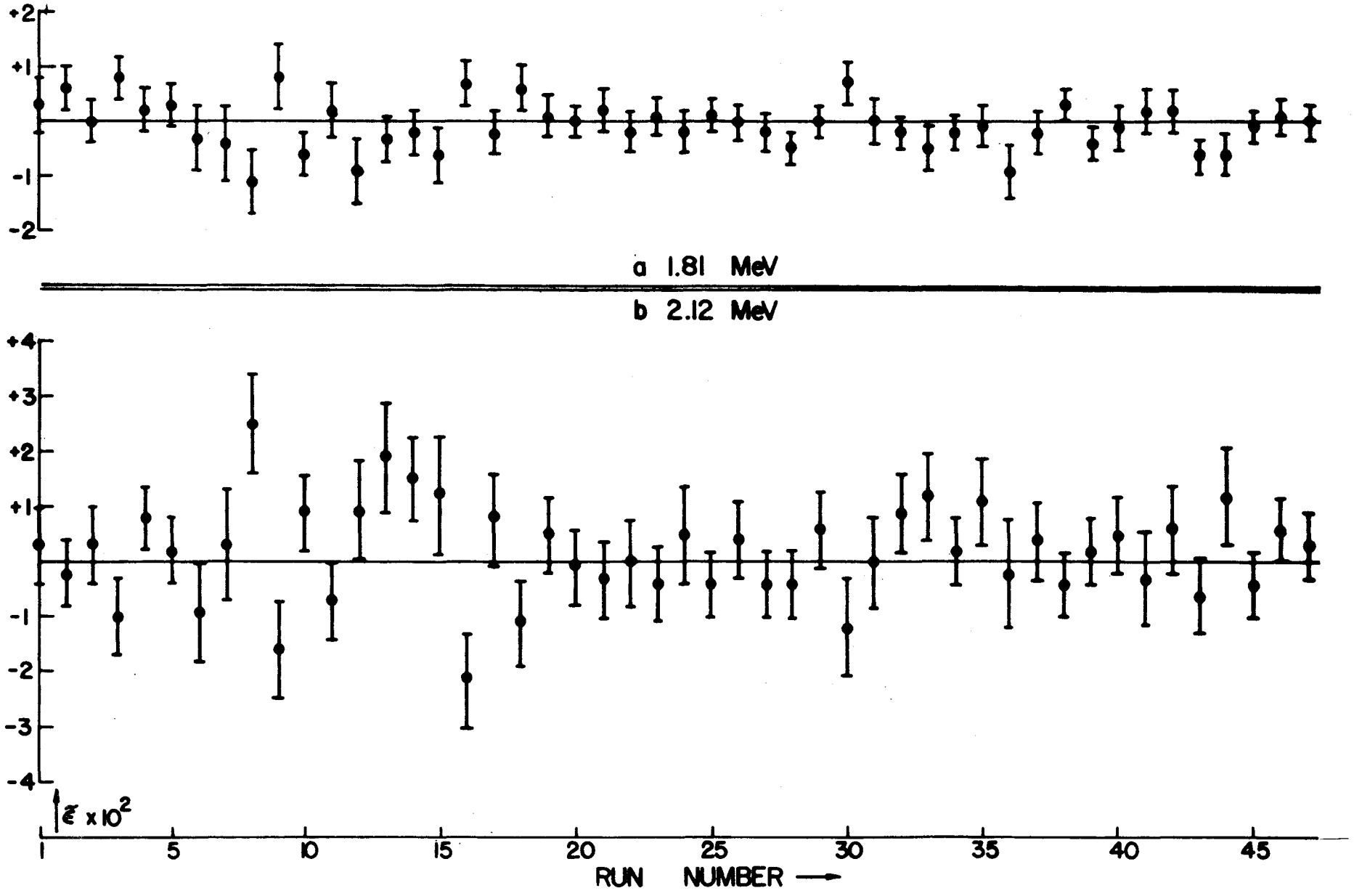
+2
+1
-1
-2
a 1.81 MeV
b 2.12 MeV
+4
+3
+2
+1
-1
-2
-3
-4
$\bar{\epsilon} \times 10^2$
1
5
10
15
20
25
30
35
40
45
RUN NUMBER ⟶

$$\chi^2(\tilde{\epsilon}_{AVG.}) = \sum_{i=1}^{\#\,runs} \frac{(\tilde{\epsilon}_i - \tilde{\epsilon}_{AVG})^2}{(\delta\tilde{\epsilon}_i)^2} \qquad (19)$$

Figure 7 illustrates the distributions of eighty-eight runs in bins of various t^2 sizes about the mean $\tilde{\epsilon}$'s. For each run

$$t_i^2 = \frac{(\tilde{\epsilon}_i - \tilde{\epsilon}_{AVG})^2}{(\delta\epsilon_i)^2} \quad . \qquad (20)$$

The plots in Figure 6 show that the $\tilde{\epsilon}$'s fluctuate randomly about zero for each run, and values of the average $\tilde{\epsilon}$'s for the 1.81 and 2.12 MeV photopeaks in Table 4 are not equal. These facts lead us to believe that our systematic errors are substantially smaller than the statistical errors.

B. Background Effects.

1. Compton Scattering. Triple coincidences from Compton scattering occur because of the following events: a) 0.845 MeV γ's arrive at the edges of the plastic detectors, scatter in the forward direction with energies $\simeq$ 0.6 MeV, and stop in the edges of the NaI Xtals; and b) 1.81 or 2.12 MeV γ's strike the NaI Xtals and scatter with energies above 0.2 MeV into the plastic scintillators, which have small but finite detection efficiencies for these γ's. By placing 1/4" thick lucite slabs between the source and β detectors, we found that Compton scattered triple coincidences amounted to about one per cent of the true triples. However, the ratio of Compton scattered triples to all triples was the same within statistics for the four types of coincidences. From the statistics, we estimated the possible error in $\tilde{\epsilon}$ due to Compton background to be less than 5×10^{-5}.

Figure 7. First eighty-eight runs in t^2 bins around $\tilde{\epsilon}_{AVG.}$.
Dotted lines show Gaussian distributions.

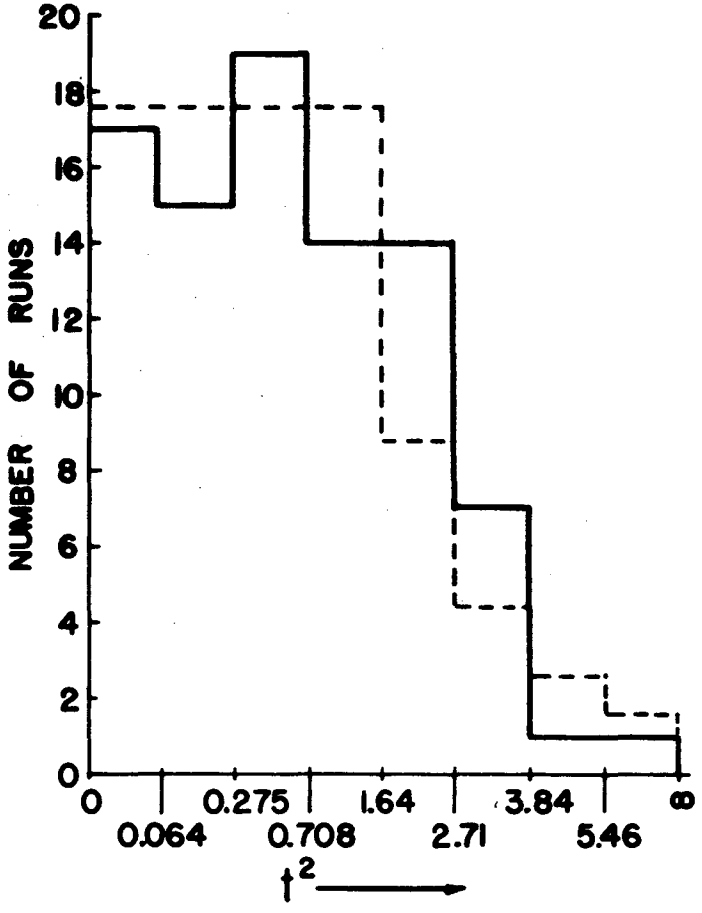

1.81 MeV

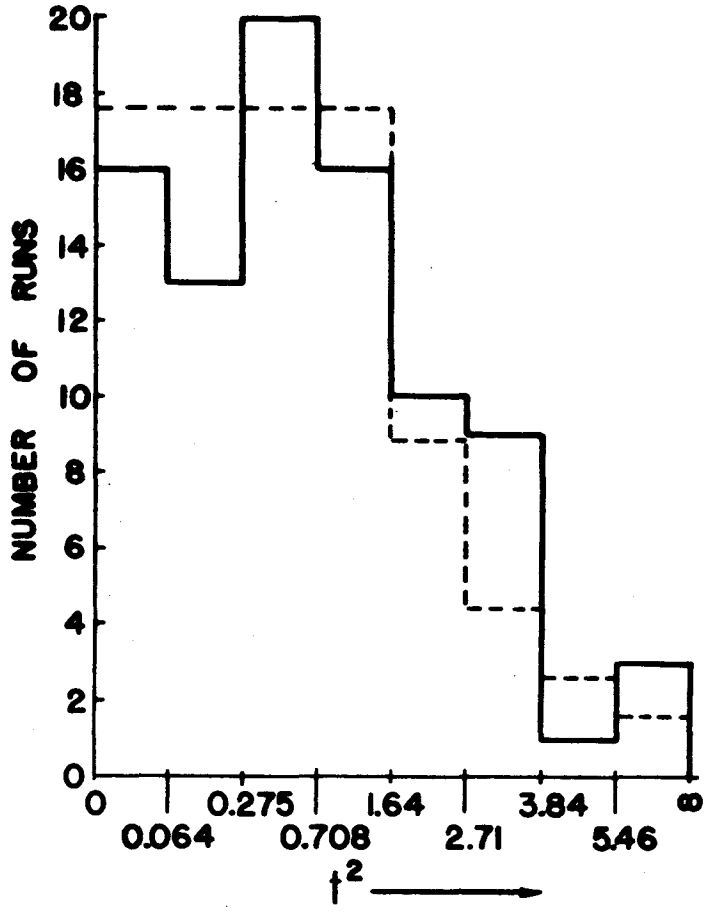

2.12 MeV

2. Na^{24} Background. Small amounts of Na^{24} (15 h) which may contribute to coincidence spectra build up in two ways during the irradiations. First, the aluminum backing on the manganese sources yields Na^{24} via (n,α). Secondly, improper handling may leave salt from the skin on the samples, which produces Na^{24} through neutron absorption. Irradiation of a test strip of one half mil aluminum foil showed that such background contributes negligibly to $\beta\gamma\gamma$ coincidences, and that it only contributes by about 0.1% to $\gamma\gamma$ coincidences when the samples are irradiated repeatedly.

C. Checks for Additional Errors.

As mentioned in Chapter IV and Appendix B, coincidence efficiencies and effects of routing (the multichannel analyzer) on pulse height spectra were checked in detail. The maximum systematic error in $\tilde{\epsilon}$ due to routing effects and deviation of E_4, the coincidence efficiency ratio of equation (9'), from unity is about 10^{-4}. These were our primary sources of systematic errors. We considered two others, however. Moving the source diagonally off center by 1/4" produced no noticeable effect in determining $\tilde{\epsilon}$, and false routing appeared to occur for less than one pulse in 10^7.

D. Normalizing by Using $\gamma\gamma$ Coincidences.

The second method of analysis of the data discussed in Chapter II should, in principle, yield two independent values of $\tilde{\epsilon}$ for each of the photopeaks. (See (13) - (16).)

$$\tilde{\epsilon}_A = \frac{U_A - 1}{U_A + 1} \qquad \text{and} \qquad \tilde{\epsilon}_B = \frac{U_B - 1}{U_B + 1} \qquad \text{where} \quad E_A = E_B = 1$$

$$\text{and } u_A = \left(N(\beta_A\gamma_{1A}\gamma_{2B})/N(\gamma_{1A}\gamma_{2B})\right)\cdot\left(N(\gamma_{2A}\gamma_{1B})/N(\beta_A\gamma_{2A}\gamma_{1B})\right) \qquad (21)$$

$$u_B = \left(N(\beta_B\gamma_{2A}\gamma_{1B})/N(\gamma_{2A}\gamma_{1B})\right)\cdot\left(N(\gamma_{1A}\gamma_{2B})/N(\beta_B\gamma_{1A}\gamma_{2B})\right) .$$

Surprisingly the average values of $\tilde{\epsilon}_A$ and $\tilde{\epsilon}_B$ for 128 runs were many standard deviations from zero for both photopeaks. However, the $\tilde{\epsilon}_A$'s and $\tilde{\epsilon}_B$'s were of opposite signs, and their averages were equal to the $\tilde{\epsilon}$'s computed by the fourfold ratio of equation (18). This seems to indicate that a systematic error was introduced by $\gamma\gamma$ normalization, which did not enter into the fourfold method. Several tests have been made to determine possible sources of such a systematic error. We first looked for background contributions by measuring coincidence count rates versus time. Plots of log (count rate) vs. time showed no curvature for three half lives. During other runs, the 0.845 MeV window of one γ detector was set well below the photopeak while the other detector continued to function normally. We hoped in that way to see if $\gamma\gamma$ background coupled with a discrepancy in window settings was responsible. No gross changes in the data were seen in this test. Finally, beta counters have now been interchanged without any alterations in routing or analysis, in order to see if the deviations in $\tilde{\epsilon}_A$ and $\tilde{\epsilon}_B$ are affected. So far, we do not have sufficient data to draw conclusions from this last test.

E. Conclusion.

According to the results of Table 4, we have found average values of $\tilde{\epsilon}$ for the 1.81 and 2.12 MeV mixed gammas of Mn^{56} to be $(3.11 \pm 2.7)\cdot 10^{-4}$ and $(6.51 \pm 5.9)\cdot 10^{-4}$ respectively. If we use a systematic error in $\tilde{\epsilon}$ of 10^{-4} imposed by the electronics, we find the values given in Table 5 for $\tilde{\epsilon}$, $(\delta\eta)$, and η. Systematic errors due to uncertainties

Table 5

Experimental Results for $\tilde{\epsilon}$, $(\delta\eta)$, and η

E	1.81 MeV	2.12 MeV
δ	0.18	-0.28
$\tilde{\epsilon}$	$(3.1 \pm 2.9) \cdot 10^{-4}$	$(6.5 \pm 6.0) \cdot 10^{-4}$
$(\delta\eta)$	$(5.9 \pm 5.5) \cdot 10^{-3}$	$(12.2 \pm 11.2) \cdot 10^{-3}$
η	$(3.3 \pm 3.0) \cdot 10^{-2}$	$(-4.3 \pm 4.0) \cdot 10^{-2}$

in counter solid angles and reduced matrix element ratios can be neglected.

The experiment gives a lower limit on time reversal invariance. If we assume that even and odd matrix elements are of normal order of magnitude, the limit on time reversal violation is $\eta \lesssim 3 \times 10^{-2}$. If, however, one assumes with Henley and Jacobsohn [13] that the odd term could be larger than expected, and that the product $(\delta\eta)$ is the important number, we get a limit of about 0.5×10^{-2}.

From our experiment, we conclude that the difficulties in using β-γ-γ correlation for testing time reversal violation are severe. The geometrical arrangement and background problems demand that data be accumulated and treated as symmetrically as possible. No matter how carefully one tries to exclude systematic errors, such factors as coincidence counting efficiencies of the electronics and effects of pulse routing on pulse height analysis will always give rise to a lower bound for the uncertainty in measuring the interference term $\tilde{\epsilon}$. With our present modular system, we estimate this lower bound to be $\mathcal{O}(10^{-4})$. Hence, for the cascades of Mn^{56}, the limiting uncertainty in measuring the phase difference η is $\mathcal{O}(10^{-2})$, and the limiting uncertainty in $(\delta\eta)$ is $\mathcal{O}(10^{-3})$. If the recent hypotheses discussed here are correct and η or $(\delta\eta) = \mathcal{O}(\alpha/2\pi) = \mathcal{O}(10^{-3})$, a $\beta\gamma\gamma$ triple coincidence experiment may not conclusively detect time reversal violation until a new generation of counters and electronics is available.

APPENDIX A. BETA-GAMMA-GAMMA CORRELATION

For the case of a pure Gamow-Teller beta decay followed by a mixed gamma transition and then by a pure transition, with nuclear spins $J \xrightarrow{\beta} J_1 \xrightarrow{\text{(mixed)}\gamma} J_2 \xrightarrow{\text{(pure)}\gamma} J_0$, DeSabbata [7] writes the angular correlation in the form

$$W_{\beta\gamma\gamma} = \sum_{k_1,k_2} \left\{ a^0_{11} \Phi^{0k_1k_2}_{l_1 l_1'} \Phi^{k_2}_{l_2 l_2} D^{0k_1k_2}_{000}(\omega_{\beta\gamma}, \omega_{\gamma\gamma}) + a^1_{11} \left(-\tfrac{1}{\sqrt{3}}\right) \times \right. \tag{A1}$$

$$\left. \times \frac{(J_1(J_1+1) - J(J+1) + 2)}{2(J(J+1))^{1/2}} \Phi^{1k_1k_2}_{l_1 l_1'} \Phi^{k_2}_{l_2 l_2} D^{1k_1k_2}_{000}(\omega_{\beta\gamma}, \omega_{\gamma\gamma}) \right\}$$

where l_1, l_1' = angular momenta of the mixed transition,

l_2 = angular momentum of the pure transition, and

a^0_{11}, a^1_{11} = coefficients which describe the $m_s = 0$ and the $m_s = \pm 1$ states, respectively, of the electron-neutrino spin triplet.

If the correlation is directional and polarizations are not observed,

k_1 and k_2 are even, and

$$\max k_1 \leq \min(2l_1, 2l_1', 2\,|l_1 - l_1'|)$$

$$\max k_2 \leq 2l_2 .$$

The Φ's and the D^{ijk}_{000}'s are shorthand notations for sums and products of various coefficients, rotational matrices, and reduced matrix elements.

$$\Phi^{k_2}_{l_2} = ((2J_2+1)(2l_2+1))^{1/2} (-)^{J_2+J_0+l_2+k_2} \overline{W} \begin{pmatrix} l_2 & k_2 & l_2 \\ J_2 & J_0 & J_2 \end{pmatrix} (-)^{l_2-1} \times \tag{A2}$$

$$\times \langle l_2\, l_2\, 1\, -1 \,|\, k_2\, 0 \rangle \; |\langle J_0 \| l_2 \| J_2 \rangle|^2$$

$$\Phi^{0 k_1 k_2}_{l_1 l_1'} = \sum_{l_1, l_1'} \left((2J_1+1)(2J_2+1)(2k_2+1)(2k_1+1)(2l_1+1)(2l_1'+1) \right)^{1/2} (-)^{l_1'-1} \times$$
$$\times \sum \begin{pmatrix} l_1 J_2 J_1 \\ l_1' J_2 J_1 \\ k_1 k_2 0 \end{pmatrix} \langle l_1 l_1' \; 1 \; -1 | k_1 0 \rangle \langle J_2 \| l_1 \| J_1 \rangle \langle J_2 \| l_1' \| J_1 \rangle^* \qquad \text{(A3)}$$

$$\Phi^{1 k_1 k_2}_{l_1 l_1'} = \sum_{l_1, l_1'} \left(3(2J_1+1)(2J_2+1)(2k_2+1)(2k_1+1)(2l_1+1)(2l_1'+1) \right)^{1/2} (-)^{l_1'-1} \times$$
$$\times \sum \begin{pmatrix} l J_2 J_1 \\ l_1' J_2 J_1 \\ k_1 k_2 1 \end{pmatrix} \langle l_1 l_1' \; 1 \; -1 | k_1 0 \rangle \langle J_2 \| l_1 \| J_1 \rangle \langle J_2 \| l_1' \| J_1 \rangle^* \qquad \text{(A4)}$$

$$D^{1 k_1 k_2}_{000} = \sum_{x_1 x_2} D^{1}_{0x}(\omega_{\beta\gamma}) (-)^{1-x} \bar{V} \begin{pmatrix} 1 & k_1 & k_2 \\ -x & 0 & x_2 \end{pmatrix} D^{k_2}_{x_2 0}(\omega_{\gamma\delta}) \qquad \text{(A5)}$$

$$D^{0 k_1 k_2}_{000} = \sum_{x_1 x_2} D^{0}_{0x}(\omega_{\beta\gamma}) (-)^{-x} \bar{V} \begin{pmatrix} 0 & k_1 & k_2 \\ -x & 0 & x_2 \end{pmatrix} D^{k_2}_{x_2 0}(\omega_{rr}) \qquad \text{(A6)}$$

The $D^{L}_{m\mu}(\omega)$ are rotation matrices as defined by Rosenfeld[12] which transform the coordinate systems of the particles one into another. The $\langle \| l_i \| \rangle$ are reduced matrix elements. Also,

$$\bar{V} \begin{pmatrix} i & k_1 & k_2 \\ -x & 0 & x_2 \end{pmatrix} = (2k_2+1)^{-1/2} (-)^{2k_1+k_2+x_2} \langle i \, k_1 \, -x \; 0 | k_2 \, -x_2 \rangle \qquad \text{(A7)}$$

and for even arguments

$$\bar{W} \begin{pmatrix} l_2 & k_2 & l_2 \\ J_2 & J_0 & J_2 \end{pmatrix} = W(l_2 k_2 J_0 J_2 | l_2 J_2) \qquad \text{(A8)}$$

$W(abcd|ef)$ and $X\begin{pmatrix} i & j & k \\ l & m & n \\ o & p & q \end{pmatrix}$ and $\langle abcd | \alpha\beta \rangle$ are Racah, Fano, and Clebsh-Gordan coefficients, respectively.

For the transition $J = 3^+ \xrightarrow{\beta} J_1 = 2^+ \xrightarrow{\gamma_1} J_2 = 2^+ \xrightarrow{\gamma_2} J_0 = 0^+$, the first gamma is mixed with $l_1, l_1' = 1$ or 2, and the second is pure with $l_2 = 2$. Then we can write

$$W_{\beta\gamma\gamma} = a_{11}^0 \sum_{\substack{k_1=0,2,4 \\ k_2=0,2,4}} \left\{ \Phi_{l_1 l_1'}^{0 k_1 k_2} \Phi_{l_2}^{k_2} D_{000}^{0 k_1 k_2}(\omega_{\beta\gamma}, \omega_{\gamma\gamma}) + \tfrac{1}{3} \frac{a_{11}'}{a_{11}^0} \times \right.$$
$$\left. \times \Phi_{l_1 l_1'}^{1 k_1 k_2} \Phi_{l_2}^{k_2} D_{000}^{1 k_1 k_2}(\omega_{\beta\gamma}, \omega_{\gamma\gamma}) \right\} . \qquad \text{(A9)}$$

Explicitly

$$\Phi_{l_2}^{k_2} = \Phi_2^{k_2} = -5\, W(2 k_2 0 2 | 2 2) \langle 2\, 2\, 1\, -1 | k_2 0 \rangle |\langle 0 \| E2 \| 2 \rangle|^2 \qquad \text{(A10)}$$

$$\Phi_{l_1 l_1'}^{0 k_1 k_2} = \sum_{l_1, l_1' = 1,2} -5 \left((2k_2+1)(2k_1+1)(2l_1+1)(2l_1'+1) \right)^{\frac{1}{2}} (-)^{l_1'} \langle l_1 l_1'\, 1\, -1 | k_1 0 \rangle \times$$
$$\times \sum \begin{pmatrix} l_1 & 2 & 2 \\ l_1' & 2 & 2 \\ k_1 & k_2 & 0 \end{pmatrix} \langle 2 \| l_1 \| 2 \rangle \langle 2 \| l_1' \| 2 \rangle^* \qquad \text{(A11)}$$

$$\Phi_{l_1 l_1'}^{1 k_1 k_2} = \sum_{l_1, l_1' = 1,2} -5 \left(3(2k_2+1)(2k_1+1)(2l_1+1)(2l_1'+1) \right)^{\frac{1}{2}} (-)^{l_1'} \langle l_1 l_1'\, 1\, -1 | k_1 0 \rangle \times$$
$$\times \sum \begin{pmatrix} l_1 & 2 & 2 \\ l_1' & 2 & 2 \\ k_1 & k_2 & 1 \end{pmatrix} \langle 2 \| l_1 \| 2 \rangle \langle 2 \| l_1' \| 2 \rangle^* \qquad \text{(A12)}$$

The reduced matrix elements may be written $\langle \| E2 \| \rangle$ for $l_i, l_i' = 2$ and $\langle \| M1 \| \rangle$ for $l_i, l_i' = 1$. Also, the ratio $a_{11}^1 / a_{11}^0 = v\beta/c$, if we assume a real interaction constant for the beta decay and ignore forbidden beta transitions.

The terms with the rotation matrices become

$$D_{000}^{0 k_1 k_2} = \sum_{x_2 = -k_2}^{k_2} D_{00}^{0}(\omega_{\beta\gamma})\, (2k_2+1)^{-\frac{1}{2}} (-)^{x_2} \langle 0 k_1 0 0 | k_2 - x_2 \rangle D_{x_2 0}^{k_2}(\omega_{\gamma\gamma}) \qquad \text{(A13)}$$
$$= (2k_2+1)^{-\frac{1}{2}} \langle 0 k_1 0 0 | k_2 0 \rangle P_{k_2}(\theta_{\gamma\gamma})$$

and

$$D^{1\,k_1 k_2}_{0\,0\,0} = \sum_{\substack{x=-1,0,1 \\ x_2=-k_2 \cdots k_2}} D^{1}_{0x}(\omega_{\beta\delta})\,(-)^{1-x+x_2}(2k_2+1)^{-1/2}\langle 1\,k_1\,-x_1\,0\,|\,k_2\,-x_2\rangle D^{k_2}_{x_2 0}(\omega_{\gamma\delta}) \,. \quad \text{(A 14)}$$

By substituting (A 10) through (A 14) into (A 9), we get

$$W_{\beta\gamma\delta} = a'_{11}\,25\,|\langle 0\|E2\|2\rangle|^2 \Bigg[\sum_{\substack{k_1=0,2,4 \\ k_2=0,2,4 \\ l_1=1,2 \\ l_1'=1,2}} \left((2k_1+1)(2k_2+1)(2l_1+1)(2l_1'+1)\right)^{1/2} \times$$

$$\times \Big\{ W(2k_2 02|22)\langle 2\,2\,1\,-1\,|\,k_2\,0\rangle\langle l_1\,l_1'\,1\,-1\,|\,k_1\,0\rangle(-)^{l_1} \sum \begin{pmatrix} l_1 & 2 & 2 \\ l_1' & 2 & 2 \\ k_1 & k_2 & 0 \end{pmatrix} \langle 2\|l_1\|2\rangle\langle 2\|l_1'\|2\rangle^* \times \quad \text{(A 15)}$$

$$\times (2k_2+1)^{-1/2}\langle 0\,k_1\,0\,0\,|\,k_2\,0\rangle P_{k_2}(\hat{r}_{\beta_1}\cdot\hat{r}_{\gamma_2}) + v_\beta/c\,\frac{1}{\sqrt{3}}\,W(2k_2 02|22)\langle 2\,2\,1\,-1\,|\,k_2\,0\rangle \times$$

$$\times \langle l_1 l_1'\,1\,-1\,|\,k_1\,0\rangle(-)^{l_1'} \sum \begin{pmatrix} l_1 & 2 & 2 \\ l_1' & 2 & 2 \\ k_1 & k_2 & 1 \end{pmatrix} \langle 2\|l_1\|2\rangle\langle 2\|l_1'\|2\rangle^* (2k_2+1)^{-1/2} \times$$

$$\times \sum_{x_2,x} D^{1}_{0x}(\omega_{\beta\gamma})\,(-)^{1-x+x_2}\langle 1\,k_1\,-x\,0\,|\,k_2\,-x_2\rangle D^{k_2}_{x_2 0}(\omega_{\gamma\delta}) \Big\} \Bigg]$$

We can simplify somewhat by extracting common factors and by noting that $\langle 1\,k_1\,-x\,0\,|\,k_2\,-x_2\rangle$ vanishes unless $-x_2 = -x$.

Then

$$W_{\beta\gamma\delta} = a^{\circ}_{11}\,25\,|\langle 0\|E2\|2\rangle|^2 \Bigg\{ \sum_{\substack{k_1,k_2 \\ l_1,l_1'}} \left((2k_1+1)(2l_1+1)(2l_1'+1)\right)^{1/2}(-)^{l_1'} \times \quad \text{(A 16)}$$

$$\times W(2k_2 02|22)\,\langle 2\,2\,1\,-1\,|\,k_2\,0\rangle\langle l_1\,l_1'\,1\,-1\,|\,k_1\,0\rangle\langle 2\|l_1\|2\rangle\langle 2\|l_1'\|2\rangle^* \times$$

$$\times \Big[\sum \begin{pmatrix} l_1 & 2 & 2 \\ l_1' & 2 & 2 \\ k_1 & k_2 & 0 \end{pmatrix} \langle 0\,k_1\,0\,0\,|\,k_2\,0\rangle P_{k_2}(\hat{r}_{\beta_1}\cdot\hat{r}_{\gamma_2}) + \frac{v_\beta}{\sqrt{3}\,c} \sum \begin{pmatrix} l_1 & 2 & 2 \\ l_1' & 2 & 2 \\ k_1 & k_2 & 1 \end{pmatrix} \langle 1\,k_1\,-x\,0\,|\,k_2\,-x\rangle D^{1}_{0x}(\omega_{\beta\gamma}) D^{k_2}_{-x\,0}(\omega_{\gamma\delta}) \Big] \Bigg\}$$

If we inspect the properties of $(-)^{l_1'} \langle l_1 l_1' 1-1 | k_1 0 \rangle X \begin{pmatrix} l_1 & 2 & 2 \\ l_1' & 2 & 2 \\ k_1 & k_2 & 1 \end{pmatrix}$, we find that the term containing the Fano coefficient $X \begin{pmatrix} l_1 & 2 & 2 \\ l_1' & 2 & 2 \\ k_1 & k_2 & 0 \end{pmatrix}$ vanishes unless $k_1 = k_2$. The term containing $X \begin{pmatrix} l_1 & 2 & 2 \\ l_1' & 2 & 2 \\ k_1 & k_2 & 1 \end{pmatrix}$ vanishes unless $l_1 \neq l_1'$. Moreover, the mixed term appears twice when the sum $\sum_{l_1, l_1' = 1,2}$ is taken and a sign change leads to the form $(\langle 2 \| l_1 \| 2 \rangle \langle 2 \| l_1' \| 2 \rangle^* - \langle 2 \| l_1 \| 2 \rangle^* \langle 2 \| l_1' \| 2 \rangle)$. We now rewrite (A 16) so as to exhibit all of these features.

$$W_{\beta\gamma} = 25 a_{11}^{\circ} \cdot (\text{PART I} + \text{PART II}) \cdot |\langle 0 \| E2 \| 2 \rangle|^2 \tag{A17}$$

$$\text{PART I} = \sum_{\substack{k_1 = 0,2,4 \\ l_1, l_1' = 1,2}} ((2k_1+1)(2l_1+1)(2l_1'+1))^{1/2} (-)^{l_1'} W(2 k_1 0 2 | 2 2) \times$$
$$\times \langle 2 2 1 -1 | k_1 0 \rangle \langle l_1 l_1' 1 -1 | k_1 0 \rangle \langle 2 \| l_1 \| 2 \rangle \langle 2 \| l_1' \| 2 \rangle^* \times$$
$$\times \langle 0 k_1 0 0 | k_1 0 \rangle P_{k_1}(\hat{k}_{\gamma_1} \cdot \hat{k}_{\gamma_2}) X \begin{pmatrix} l_1 & 2 & 2 \\ l_1' & 2 & 2 \\ k_1 & k_1 & 0 \end{pmatrix}$$

$$\text{PART II} = \sum_{\substack{k_1 = 0,2,4 \\ k_2 = 0,2,4 \\ x = -1,0,1}} \sqrt{5} \; v_{\ell/c} (2k_1+1)^{1/2} W(2 k_2 0 2 | 2 2) \langle 2 2 1 -1 | k_2 0 \rangle \times$$
$$\times \langle 1 2 1 -1 | k_1 0 \rangle \langle 1 \; k_1 - x \; 0 | \; k_2 - x \rangle D'_{0x}(\omega_{\beta\gamma}) D^{k_2}_{-x\,0}(\omega_{\delta\delta}) \times$$
$$\times X \begin{pmatrix} 1 & 2 & 2 \\ 2 & 2 & 2 \\ k_1 & k_2 & 1 \end{pmatrix} \left\{ \langle 2 \| M1 \| 2 \rangle \langle 2 \| E2 \| 2 \rangle^* - \langle 2 \| E2 \| 2 \rangle \langle 2 \| M1 \| 2 \rangle^* \right\}$$

We now define the complex reduced matrix element ratio as

$$\delta = \langle 2 \| E2 \| 2 \rangle / \langle 2 \| M1 \| 2 \rangle \tag{A18}$$

and divide (A17) by $|\langle 2 \| M1 \| 2 \rangle|^2$.

Then, in PART I there are the following terms:

a) a mixed M1-E2 term in $(\delta + \delta^*)/2 = \mathrm{Re}(\delta)$, which is multiplied by the LeGendre polynomial $P_2(\hat{k}_{\gamma_1} \cdot \hat{k}_{\gamma_2})$,

b) pure M1 terms $\left(|\langle 2 \| M1 \| 2 \rangle|^2 / |\langle 2 \| M1 \| 2 \rangle|^2 = 1\right)$ which are multiplied by LeGendre polynomials P_0 and P_2, and

c) pure E2 terms in $|\delta|^2$ which are multiplied by P_0, P_2, and P_4.

PART II contains a mixed term in $-i(\delta^* - \delta)/2 = -\mathrm{Im}(\delta)$.

For convenience, we can also divide (A17) by $25\, a_{11}^0\, |\langle 0 \| E2 \| 2 \rangle|^2$ times the coefficient of the $k_1 = 0$, $1_1 = 1_1' - 1$ term in PART I.

Henley and Jacobsohn[5] carried out the evaluation for the cascade, and obtained the result

$$W_{\beta\gamma\gamma} = W_{\beta\gamma\gamma} \Big/ \left(25\, a_{11}^0\, |\langle 0 \| E2 \| 2 \rangle|^2\, |\langle 2 \| M1 \| 2 \rangle|^2\, (-)\sqrt{3/5}\; W(2002|22) X\begin{pmatrix} 1 & 2 & 2 \\ 1 & 2 & 2 \\ 0 & 0 & 0 \end{pmatrix}\right) \tag{A19}$$

$$= 1 + |\delta|^2 + \left(0.250 + 0.732\left(\frac{\delta^* + \delta}{2}\right) + 0.0765\,|\delta|^2\right) P_2(\hat{k}_{\gamma_1} \cdot \hat{k}_{\gamma_2})$$

$$+ 0.327\,|\delta|^2\, P_4(\hat{k}_{\gamma_1} \cdot \hat{k}_{\gamma_2}) - 0.245\, v/c\; i\left(\frac{\delta^* - \delta}{2}\right) \hat{k}_\beta \cdot (\hat{k}_{\gamma_1} \times \hat{k}_{\gamma_2})(\hat{k}_{\gamma_1} \cdot \hat{k}_{\gamma_2}) \ .$$

As in the previous discussion, the $\hat{k}$'s are unit vectors in the directions of the outgoing particles. The reader will note that, according to the definition above, the total probability for $\beta\gamma\gamma$ emission over all angles is

$$\int W_{\beta\gamma\gamma}\, d\Omega_\beta d\Omega_{\gamma\gamma} = 1 + |\delta|^2 \ . \tag{A20}$$

APPENDIX B. ELECTRONICS

The basic electronics has been discussed in Chapter IV. Here, we treat several aspects of the system in more detail.

1. Fast Coincidence Circuitry.

Figure 1 - A. shows the fast coincidence circuitry with important delays t_{An}, τ, t_w, and T. All other delays caused by connecting cables and by the characteristics of the triggers, coincidence circuits, etc. have been left out for the sake of simplicity. Only one β detector is shown. Delay times, pulse widths, and energy thresholds are given in Table 1 - A.

Anode pulses corresponding to gamma energies greater than $\simeq 0.15$ MeV cause the anode triggers to fire short logic pulses. Whenever anode trigger pulses, delayed by t_{An}, are in coincidence with long logic pulses from the Dy 12 triggers (which have thresholds corresponding to gamma energies greater than $\simeq 0.50$ MeV) the appropriate AnDy coincidence circuit fires. By putting an open cable, whose length corresponds to a $\tau/2$ delay, on the AnDy A coincidence circuit, two short logic pulses τ apart are generated for each anode-dynode coincidence. AnDy B, operating in normal fashion, fires once per anode-dynode coincidence. Timing is arranged so that an AnDy B pulse is in true coincidence with the first AnDy A pulse and in false coincidence with the second. Because the delay time τ is well outside the resolving time of the $\gamma_A\gamma_B$ fast coincidence circuit, the number of such false events that occur within the course of a run should statistically correspond to the number of accidental $\gamma_A\gamma_B$ coincidences which are inseparable from true coincidences. This will be true to the extent that the resolving time for the false pulse coincidences is identical to the resolving time for the true pulse coincidences.

Table 1 - A.

Typical Delays, Pulse Widths, and Thresholds

Pulse or Delay	Width nsec	Trigger	Threshold (MeV)
t_{An}	25	An (A,B)	0.15
τ	50	Dy 12 (A,B)	0.50
T	325	Lowest Level γ (A,B) Storage	1.30
t_w	29	Upper Level γ (A,B) Window	0.95
Dy 12 (A,B)	36		
An (A,B)	6	Lower Level γ (A,B) Window	0.55
AnDy B	6		
AnDy A, AnDy A del.	6.6	Lowest β (A,B) Disc. Level	0.10
$\gamma_A \gamma_B$	8	Lower Level β (A,B) Disc. Window	0.20
β_A, β_B	8.5		
$\gamma\gamma$, $\gamma\gamma$ del.	8.5	Upper Level β (A,B) Disc.	0.95
$(\gamma\gamma)\beta_A$, $(\gamma\gamma)\beta_B$	8	Disc.	
Wide A	50		
Wide False $\gamma_A \gamma_B$	50		

Figure 1 - A. Fast coincidence circuit and important delays.

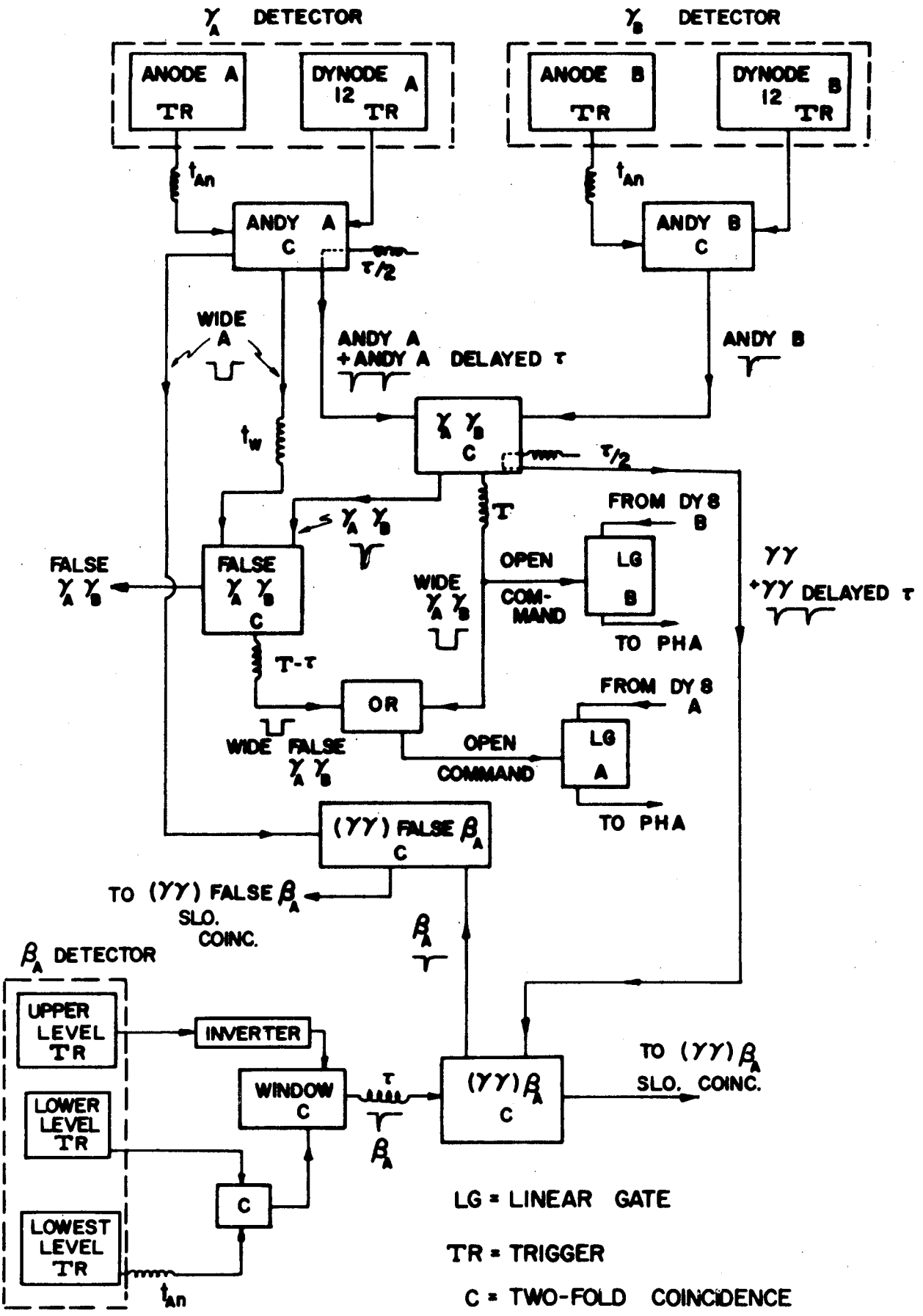
γ_A DETECTOR
γ_B DETECTOR
ANODE A TR
DYNODE 12 A TR
ANODE B TR
DYNODE 12 B TR
t_{An}
ANDY A C
ANDY B C
$\tau/2$
WIDE A
ANDY A + ANDY A DELAYED τ
ANDY B
t_w
$\gamma_A\gamma_B$ C
$\tau/2$
T
FROM DY 8 B
FALSE $\gamma_A\gamma_B$
FALSE $\gamma_A\gamma_B$ C
WIDE $\gamma_A\gamma_B$
OPEN COMMAND
LG B
TO PHA
$\gamma\gamma$ + $\gamma\gamma$ DELAYED τ
$T-\tau$
OR
FROM DY 8 A
WIDE FALSE $\gamma_A\gamma_B$
OPEN COMMAND
LG A
TO PHA
$(\gamma\gamma)$ FALSE β_A C
TO $(\gamma\gamma)$ FALSE β_A SLO. COINC.
β_A
β_A DETECTOR
UPPER LEVEL TR
INVERTER
WINDOW C
τ
β_A
$(\gamma\gamma)\beta_A$ C
TO $(\gamma\gamma)\beta_A$ SLO. COINC.
LOWER LEVEL TR
C
LOWEST LEVEL TR
t_{An}
LG = LINEAR GATE
TR = TRIGGER
C = TWO-FOLD COINCIDENCE

We have measured these resolving times and have seen that they differ by less than one half per cent. Since the ratio of false to true coincidences is $\mathcal{O}(10^{-2})$, this would cause a negligible systematic error in the determination of the interference term in the correlation.

Note the distinction (in the above) between true, accidental, and false coincidences. The first two are inseparable, but the last type is manufactured by the circuitry in order to measure the second.

The false $\gamma_A\gamma_B$ coincidence circuit fires only when a $\gamma_A\gamma_B$ coincidence pulse is sufficiently late to be in coincidence with a subsidiary wide pulse (delayed by t_w) from AnDy A, i.e., the false $\gamma_A\gamma_B$ coincidence circuit fires only when an AnDy B pulse is in coincidence with the second AnDy A pulse.

If a $\gamma\gamma$ coincidence is present, any analysis of it will be subjected to address modification or routing according to whether it was a false or true coincidence by determining whether the second most significant binary bit in the address register is 0 or 1. We have arranged this address modification so that the false $\gamma_A\gamma_B$ pulses are advanced four groups in the pulse height analyzer storage unit. A total of sixteen groups is available in the multichannel analyzer. We have observed the effect of routing which precedes pulse height analysis on that analysis and found the areas under our photopeaks to be affected by less than one part in 10^{-4}.

A second measure of accidental events is provided by the $\gamma_A\gamma_B$ coincidence circuit, which sends two pulses, separated by τ, to the $\beta_A(\gamma\gamma)$ fast coincidence circuit for every $\gamma_A\gamma_B$ (or delayed $\gamma_A\gamma_B$) coincidence. These separated pulses are denoted $\gamma\gamma$ and $\gamma\gamma$ delayed. Since the short logic pulses which correspond to $0.20\ \text{MeV} \lesssim E_\beta \lesssim 0.95\ \text{MeV}$ are effectively delayed $\tau + t_{An}$, a true $\beta_A\gamma\gamma$ coincidence will give rise

to an overlap of the β logic pulse with the delayed $\gamma\gamma$ pulse. If the β pulse overlaps the first of the $\gamma\gamma$ pulses, the $\beta\gamma\gamma$ coincidence is false, and this fact is discovered by the ($\gamma\gamma$) false β_A coincidence circuit, which sees a γ_A input that is not delayed by τ . Both $(\gamma\gamma)\beta_A$ and ($\gamma\gamma$) false β_A coincidence circuits fire slow coincidence circuits; the slow circuits, in turn, route pulses from ($\gamma\gamma$) β_A and ($\gamma\gamma$) false β_A events by one and seven groups respectively in the multichannel analyzer.

True and false pulses of all types are included in Figures 2a - A. and 2b - A. γ_A and γ_B on the figures are pulses from the AnDy circuits. In order to explain the routing of events by eight or more groups, it should be recalled that energy discriminators (Figure 5) differentiate between the two events, $\gamma_{1A}\gamma_{2B}$ and $\gamma_{2A}\gamma_{1B}$. In the first event, a 1.81 or 2.12 MeV γ (i.e. γ_1) is counted by detector γ_A at the same time that a 0.845 MeV γ (i.e. γ_2) is counted by detector γ_B . In the second event, the gammas play opposite roles. $\gamma_{1A}\gamma_{2B}$ events give rise to no routing signals due to the energy discriminators, but $\gamma_{2A}\gamma_{1B}$ events are routed eight groups into the second half of the analyzer.

One delay not mentioned so far is T, which depends on the clipping time of the double delay line amplifiers that amplify eighth dynode pulses of the γ counters. We allow the amplified pulses to peak before opening linear gates and taking 50 nsec samples by means of the wide $\gamma_A\gamma_B$ pulses. Since we wish to open the linear gates at the same time relative to the anode triggers for false and true $\gamma_A\gamma_B$ coincidences, the wide false $\gamma_A\gamma_B$ pulse is delayed by T - τ , and the $\gamma_A\gamma_B$ pulse is delayed by T.

2. Coincidence Efficiencies.

Accurate delay curves were obtained before the experiment by measuring coincidence efficiencies as functions of variable delays in

Figure 2a - A. Fast coincidences (1) through (3) for routing. τ = 50 nanoseconds. t = 10 nanoseconds. Table applies to cases (1) through (6) inclusive.

(1) TRUE $\gamma\gamma$

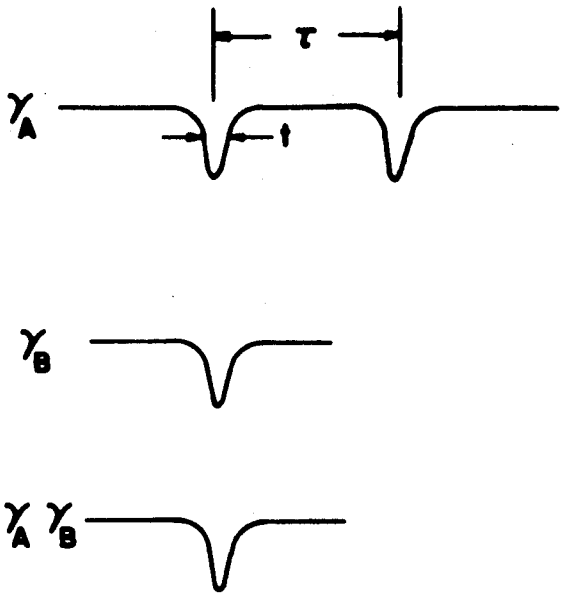

(2) FALSE $\gamma\gamma$

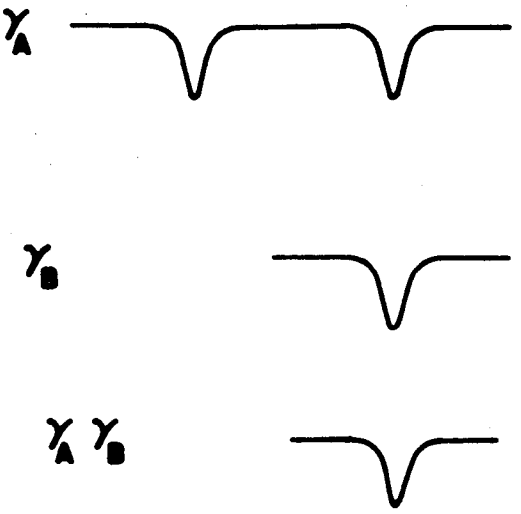

(3) TRUE $\beta(\gamma\gamma)$

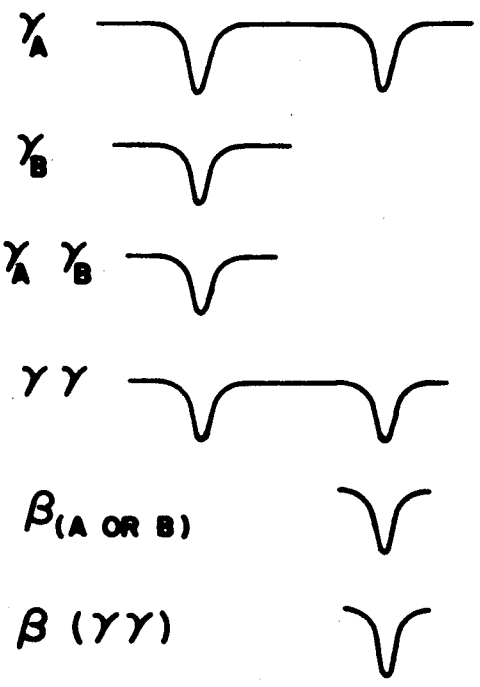

IF	ROUTE
(1) BUT NOT (3), NOT (4)	0 OR 8
(2) BUT NOT (5), NOT (6)	4 OR 12
(3) AND (1)	1 OR 2 9 OR 10
(4) AND (1)	3 OR 7 11 OR 15
(5) OR (6) AND (2)	5 OR 6 13 OR 14

Figure 2b - A. Fast coincidences (4) through (6) for routing.

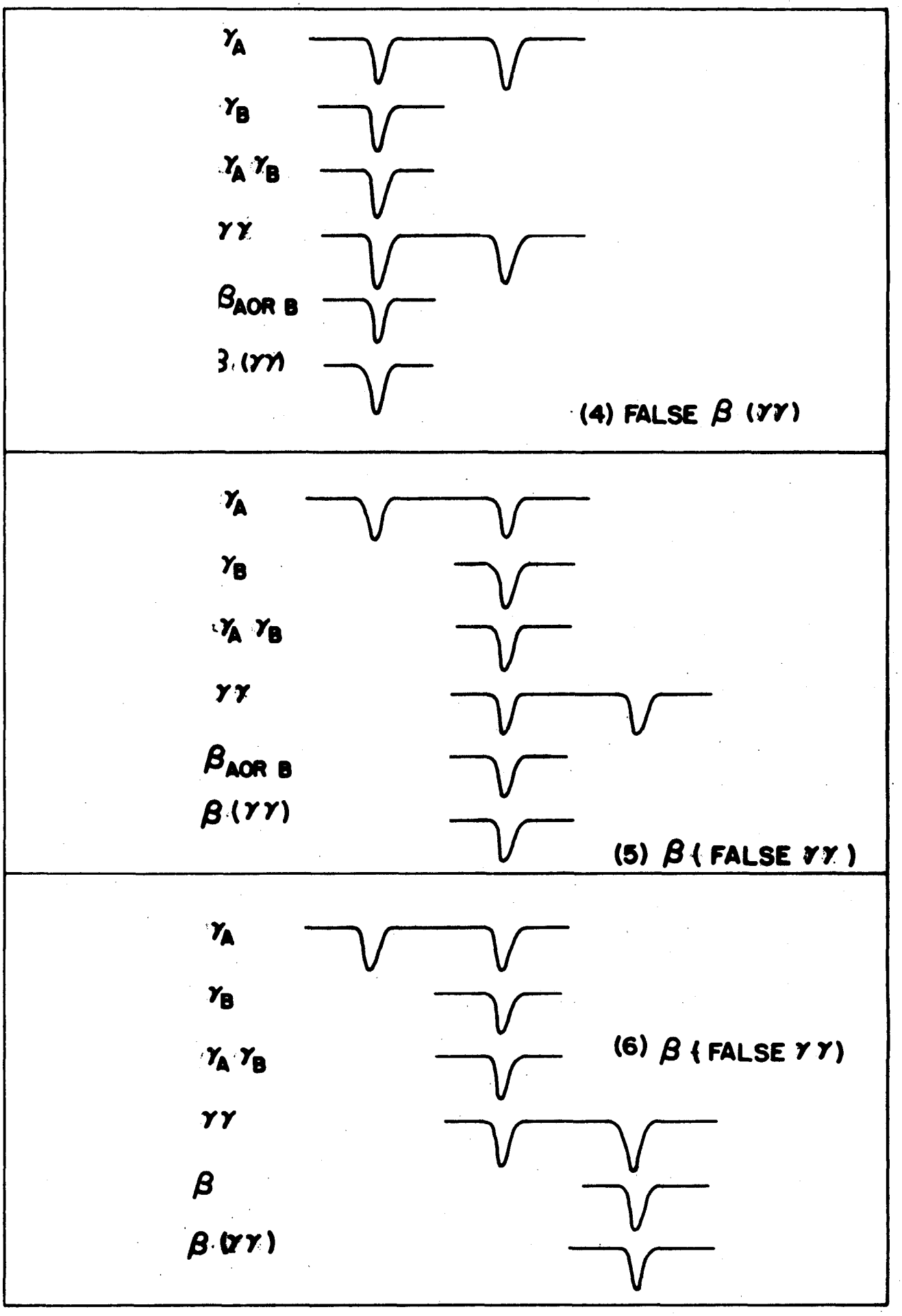
γ_A
γ_B
$\gamma_A\,\gamma_B$
$\gamma\gamma$
$\beta_{A\,OR\,B}$
$\beta\,(\gamma\gamma)$
(4) FALSE β $(\gamma\gamma)$
γ_A
γ_B
$\gamma_A\,\gamma_B$
$\gamma\gamma$
$\beta_{A\,OR\,B}$
$\beta\,(\gamma\gamma)$
(5) β { FALSE $\gamma\gamma$ }
γ_A
γ_B
$\gamma_A\,\gamma_B$
$\gamma\gamma$
β
$\beta\,(\gamma\gamma)$
(6) β { FALSE $\gamma\gamma$ }

the system. Periodically during the experiment we checked the coincidence efficiencies to make sure that our circuits continued to operate at the same points on the delay curves within 0.7 nsec. In order to obtain accurate measurements of coincidence efficiencies we tested each important coincidence circuit with one input pulse at least twice as wide as normal and compared the performance using the wide input with normal performance. This was done, in practice, by inserting a parallel coincidence circuit, which was fed the altered input, into the system. Fast coincidences in the normally operating circuit were registered as fast coincidences in the "wide" circuit, but any coincidences in the wide circuit which failed to register as fast coincidences in the normal circuit showed that the normal circuit was not completely efficient. By making use of the analyzer routing, we tested coincidence efficiencies in this fashion to four parts in 10^4.

3. Miscellaneous Tests.

As a check on the stability of the γ counters and amplifiers, we printed out coincidence pulse height spectra from the photomultiplier tubes before and after each run, observed the photopeak positions, and adjusted the threshold settings of the triggers in the gamma energy discriminators whenever necessary. From time to time, the levels of the beta discriminators were also checked using two conversion electron sources, Bi^{207} and Cs^{137}, and suitable pulse attenuators. During the course of each run logic pulses were scaled from various triggers and coincidence circuits. Any gross malfunctions, e.g., a trigger that latched or double-fired, could be quickly observed by means of the scalers.

APPENDIX C. DATA PROCESSING

Here we present a detailed description of the data analysis and show the results for a typical run in Table 2-A.

1. Correcting for Accidental Coincidences.

Multichannel analyzer displays for Run #47 are exhibited in Figures 3a - A. through 3d - A. If we assume false coincidence spectra to correspond to accidentals of various types, then from the data stored in the first half of the analyzer, we get

$$\text{True } \gamma_{1A}\gamma_{2B}\beta_A = T_{\gamma_{1A}}T_{\gamma_{2B}}T_{\beta_A} = ① - ⑦ - ⑤ + 2F_{\gamma_{1A}}F_{\gamma_{2B}}F_{\beta_A}$$

$$\text{True } \gamma_{1A}\gamma_{2B}\beta_B = T_{\gamma_{1A}}T_{\gamma_{2B}}T_{\beta_B} = ② - ③ - ⑥ + 2F_{\gamma_{1A}}F_{\gamma_{2B}}F_{\beta_B} \qquad \text{(A21)}$$

$$\text{True } \gamma_{1A}\gamma_{2B} = T_{\gamma_{1A}}T_{\gamma_{2B}} = ⓪ + ① + ② + ③ + ⑦ - (④ + ⑤ + ⑥)$$

$$\text{Accidental } \gamma_{1A}\gamma_{2B} = F_{\gamma_{1A}}F_{\gamma_{2B}} = ④ + ⑤ + ⑥$$

F and T stand for false and true coincidences, the subscripts indicate the particle observed and the detector that detected it, and the circles stand for corresponding groups in the multichannel analyzer. From the data stored in the second half of the analyzer, we obtain numbers of true $\gamma_{1B}\gamma_{2A}\beta_A$ triples, true $\gamma_{1B}\gamma_{2A}$ doubles, true $\gamma_{1B}\gamma_{2A}\beta_B$ triples and accidental $\gamma_{1B}\gamma_{2A}$ doubles. The forms are the same, except that each circled number in (A21) is increased by eight, e.g.

$$\text{True } \gamma_{1B}\gamma_{2A}\beta_A = T_{\gamma_{1B}}T_{\gamma_{2A}}T_{\beta_A} = ⑨ - ⑮ - ⑬ + 2F_{\gamma_{1B}}F_{\gamma_{2A}}F_{\beta_A}$$

Table 2 - A.

Counts Accumulated and Ratios for One Run (Run No. 47)

Parentheses Indicate Powers of Ten

COUNTS ACCUMULATED

	Group	1.81 MeV	1.81 MeV Group i / Group 0	2.12 MeV	2.12 MeV Group i / Group 0
0	$\gamma_{1A}\gamma_{2B}$	3.90 (5)	1	1.43 (5)	1
1	$\beta_A\gamma_{1A}\gamma_{2B}$	6.62 (4)	1.70 (-1)	2.00 (4)	1.40 (-1)
2	$\beta_B\gamma_{1A}\gamma_{2B}$	6.69 (4)	1.71 (-1)	2.01 (4)	1.41 (-1)
3	$F\beta_B(\gamma_{1A}\gamma_{2B})$	4.17 (2)	1.07 (-3)	1.30 (2)	0.91 (-3)
4	$(F\gamma_{1A}\gamma_{2B})$	2.64 (3)	6.75 (-3)	1.14 (3)	7.95 (-3)
5	$\beta_A(F\gamma_{1A}\gamma_{2B})$	7.88 (2)	2.02 (-3)	3.16 (2)	2.21 (-3)
6	$\beta_B(F\gamma_{1A}\gamma_{2B})$	8.39 (2)	2.15 (-3)	3.07 (2)	2.05 (-3)
7	$F\beta_A(\gamma_{1A}\gamma_{2B})$	4.15 (2)	1.06 (-3)	1.41 (2)	0.99 (-3)
	First Half				
	Second Half Normalize Using Group 8				
8	$\gamma_{2A}\gamma_{1B}$	3.94 (5)	1	1.44 (5)	1
9	$\beta_A\gamma_{2A}\gamma_{1B}$	6.72 (4)	1.72 (-1)	2.04 (4)	1.42 (-1)
10	$\beta_B\gamma_{2A}\gamma_{1B}$	6.80 (4)	1.73 (-1)	2.03 (4)	1.41 (-1)
11	$F\beta_B(\gamma_{2A}\gamma_{1B})$	4.16 (2)	1.06 (-3)	1.58 (2)	1.09 (-3)
12	$(F\gamma_{2A}\gamma_{1B})$	2.63 (3)	6.68 (-3)	1.10 (3)	7.65 (-3)
13	$\beta_A(F\gamma_{2A}\gamma_{1B})$	7.44 (2)	1.89 (-3)	2.47 (2)	1.72 (-3)
14	$\beta_B(F\gamma_{2A}\gamma_{1B})$	7.75 (2)	1.97 (-3)	2.87 (2)	1.99 (-3)
15	$F\beta_A(\gamma_{2A}\gamma_{1B})$	3.75 (2)	0.95 (-3)	1.29 (2)	0.90 (-3)

(over)

COUNTS ACCUMULATED (cont'd.)

Type of Event	1.81 MeV	2.12 MeV
$T_{\delta_{1A}} T_{\gamma_{2B}}$	5.20 (5)	1.82 (5)
$\overline{T_{\gamma_{1A}} T_{\gamma_{2B}}}$	4.07 (5)	1.29 (5)
$T_{\gamma_{2A}} T_{\gamma_{1B}}$	5.26 (5)	1.83 (5)
$\overline{T_{\gamma_{2A}} T_{\gamma_{1B}}}$	4.29 (5)	1.29 (5)
$T_{\beta_A} T_{\gamma_{1A}} T_{\gamma_{2B}}$	6.51 (4)	1.96 (4)
$\overline{T_{\beta_A} T_{\gamma_{1A}} T_{\gamma_{2B}}}$	5.40 (4)	1.26 (4)
$T_{\beta_B} T_{\gamma_{1A}} T_{\gamma_{2B}}$	6.56 (4)	1.96 (4)
$\overline{T_{\beta_B} T_{\gamma_{1A}} T_{\gamma_{2B}}}$	5.46 (4)	1.26 (4)
$T_{\beta_A} T_{\gamma_{2A}} T_{\gamma_{1B}}$	6.61 (4)	2.00 (4)
$\overline{T_{\beta_A} T_{\gamma_{2A}} T_{\gamma_{1B}}}$	5.64 (4)	1.29 (4)
$T_{\beta_B} T_{\gamma_{2A}} T_{\gamma_{1B}}$	6.68 (4)	1.99 (4)
$\overline{T_{\beta_B} T_{\gamma_{2A}} T_{\gamma_{1B}}}$	5.73 (4)	1.27 (4)

RATIOS AND $\tilde{\epsilon}$'s	(No parentheses used here to indicate powers of ten)	
u	1.0054	0.9823
u_A	1.0098	0.9740
u_B	0.9956	1.0085
$\tilde{\epsilon}$	$(0.134 \pm 0.288) \cdot 10^{-2}$	$(-0.447 \pm 0.647) \cdot 10^{-2}$
$\tilde{\epsilon}_A$	$(0.489 \pm 0.343) \cdot 10^{-2}$	$(-1.32 \pm 0.770) \cdot 10^{-2}$
$\tilde{\epsilon}_B$	$(-0.221 \pm 0.340) \cdot 10^{-2}$	$(0.422 \pm 0.778) \cdot 10^{-2}$

Figure 3a - A. Typical coincidence data stored in multichannel for one run. Groups 0 through 3. 1.81 MeV photopeak analysis uses channels 44-52. 2.12 MeV photopeak analysis uses channels 53-61.

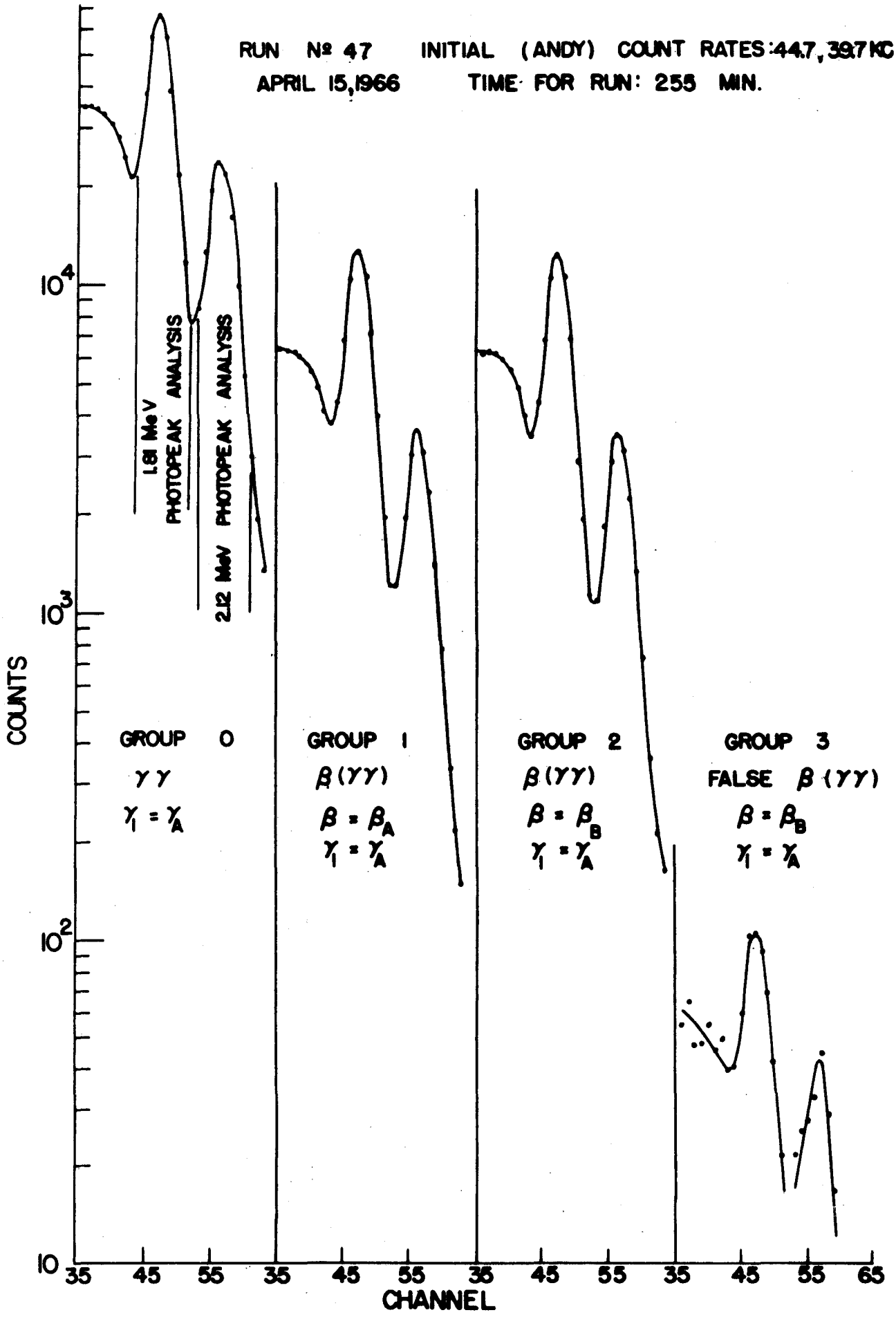
RUN Nº 47 INITIAL (ANDY) COUNT RATES: 44.7, 39.7 KC
APRIL 15, 1966 TIME FOR RUN: 255 MIN.
1.81 MeV PHOTOPEAK ANALYSIS
2.12 MeV PHOTOPEAK ANALYSIS
GROUP 0
γ γ
γ1 = γA
GROUP 1
β (γγ)
β = βA
γ1 = γA
GROUP 2
β (γγ)
β = βB
γ1 = γA
GROUP 3
FALSE β (γγ)
β = βB
γ1 = γA
COUNTS
10
10²
10³
10⁴
35
45
55
35
45
55
35
45
55
35
45
55
65
CHANNEL

Figure 3b - A. Typical coincidence data stored in multichannel for one run. Groups 4 through 7. 1.81 MeV photopeak analysis uses channels 44-52. 2.12 MeV photopeak analysis uses channels 53-61.

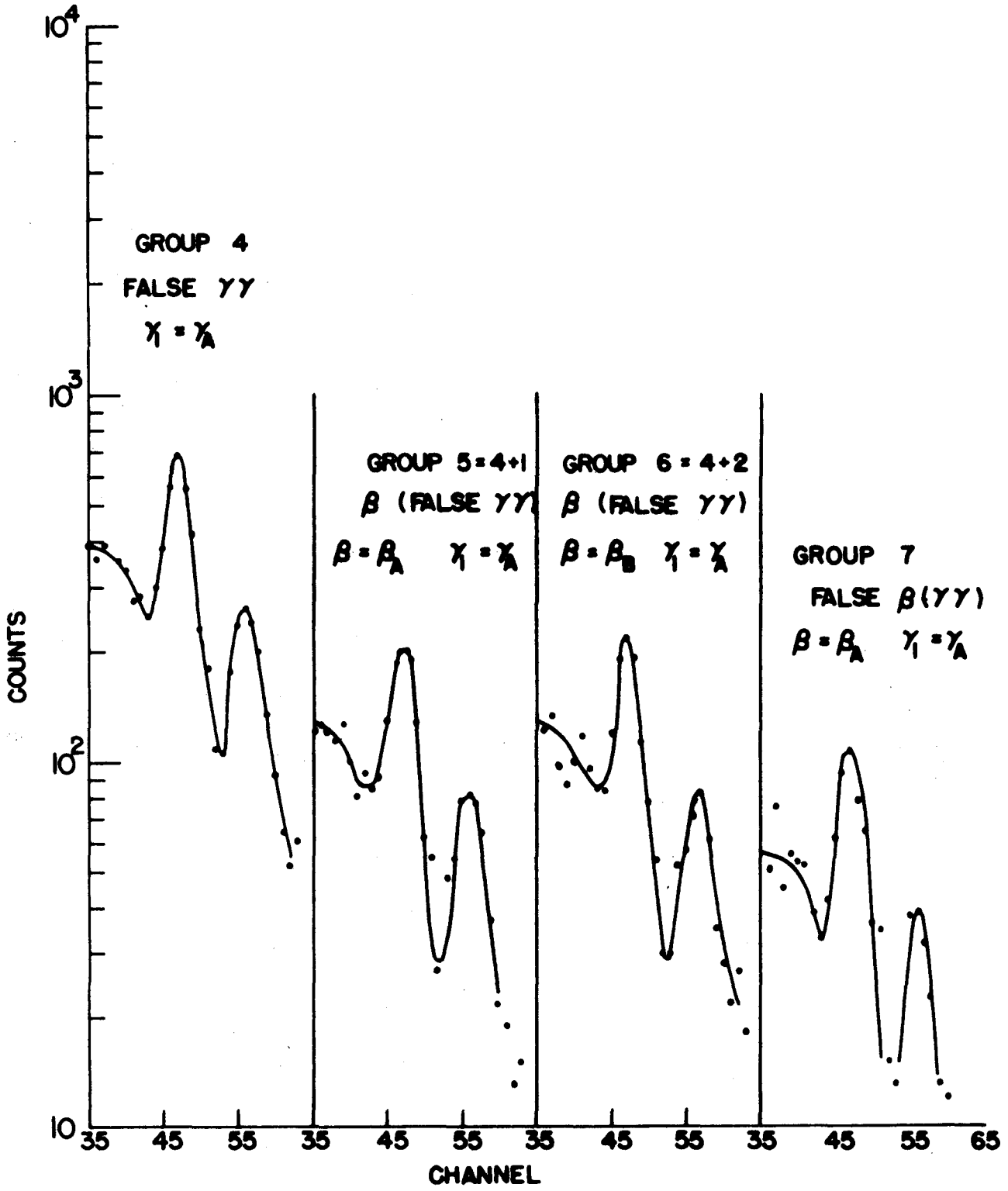
10^4
10^3
10^2
10
COUNTS
GROUP 4
FALSE γγ
$\gamma_1 = \gamma_A$
GROUP 5 = 4+1
β (FALSE γγ)
$\beta = \beta_A$ $\gamma_1 = \gamma_A$
GROUP 6 = 4+2
β (FALSE γγ)
$\beta = \beta_B$ $\gamma_1 = \gamma_A$
GROUP 7
FALSE β(γγ)
$\beta = \beta_A$ $\gamma_1 = \gamma_A$
35 45 55 35 45 55 35 45 55 35 45 55 65
CHANNEL

Figure 3c - A. Typical coincidence data stored in multichannel for one run. Groups 8 through 11. 1.81 MeV photopeak analysis uses channels 42-50. 2.12 MeV photopeak analysis uses channels 51-59.

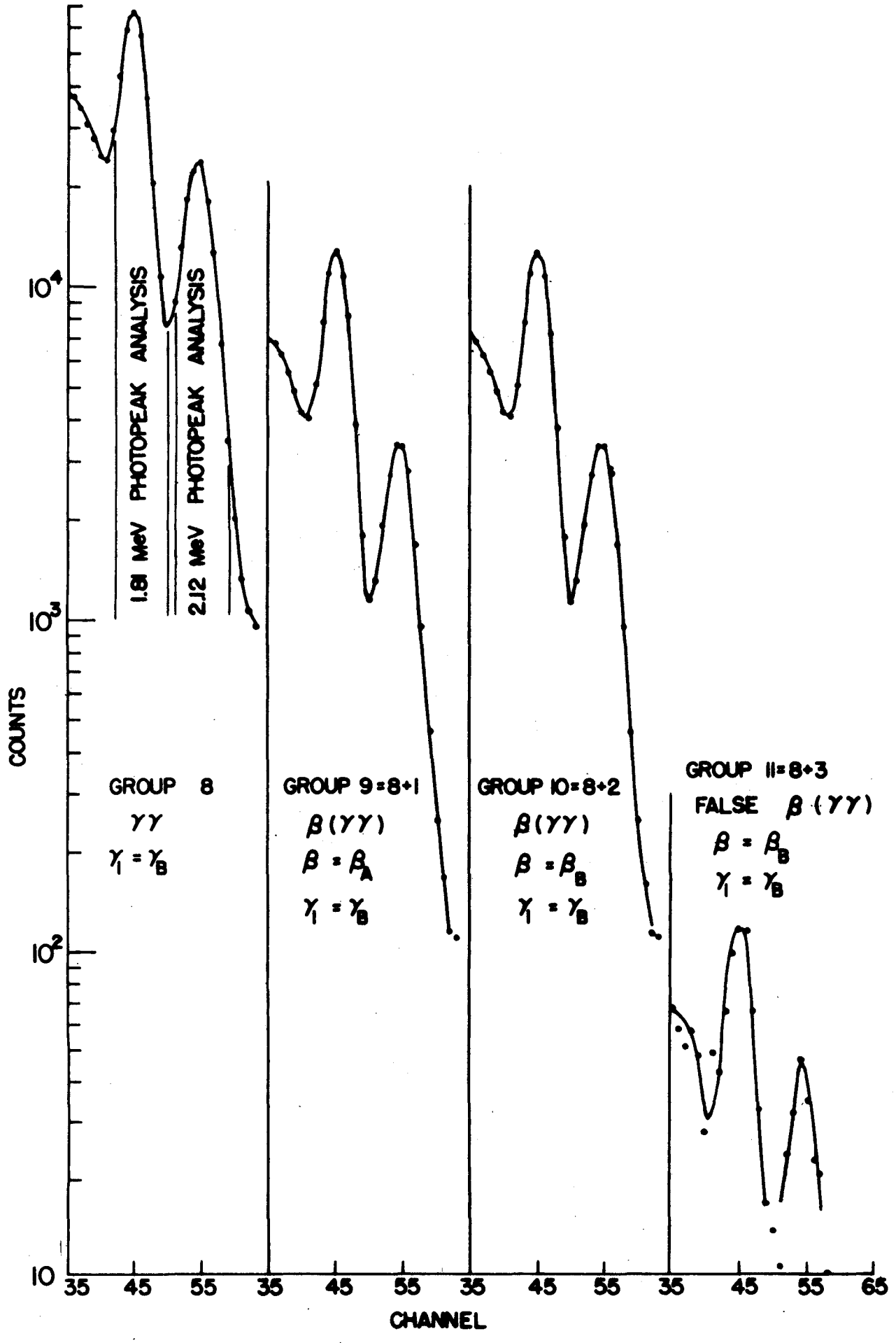
1.81 MeV PHOTOPEAK ANALYSIS
2.12 MeV PHOTOPEAK ANALYSIS
GROUP 8
γγ
γ1 = γB
GROUP 9=8+1
β(γγ)
β = βA
γ1 = γB
GROUP 10=8+2
β(γγ)
β = βB
γ1 = γB
GROUP 11=8+3
FALSE β(γγ)
β = βB
γ1 = γB
COUNTS
CHANNEL
10
10²
10³
10⁴
35
45
55
65

Figure 3d - A. Typical coincidence data stored in multichannel for one run. Groups 12 through 15, 1.81 MeV photopeak analysis uses channels 42-50. 2.12 MeV photopeak analysis uses channels 51-59.

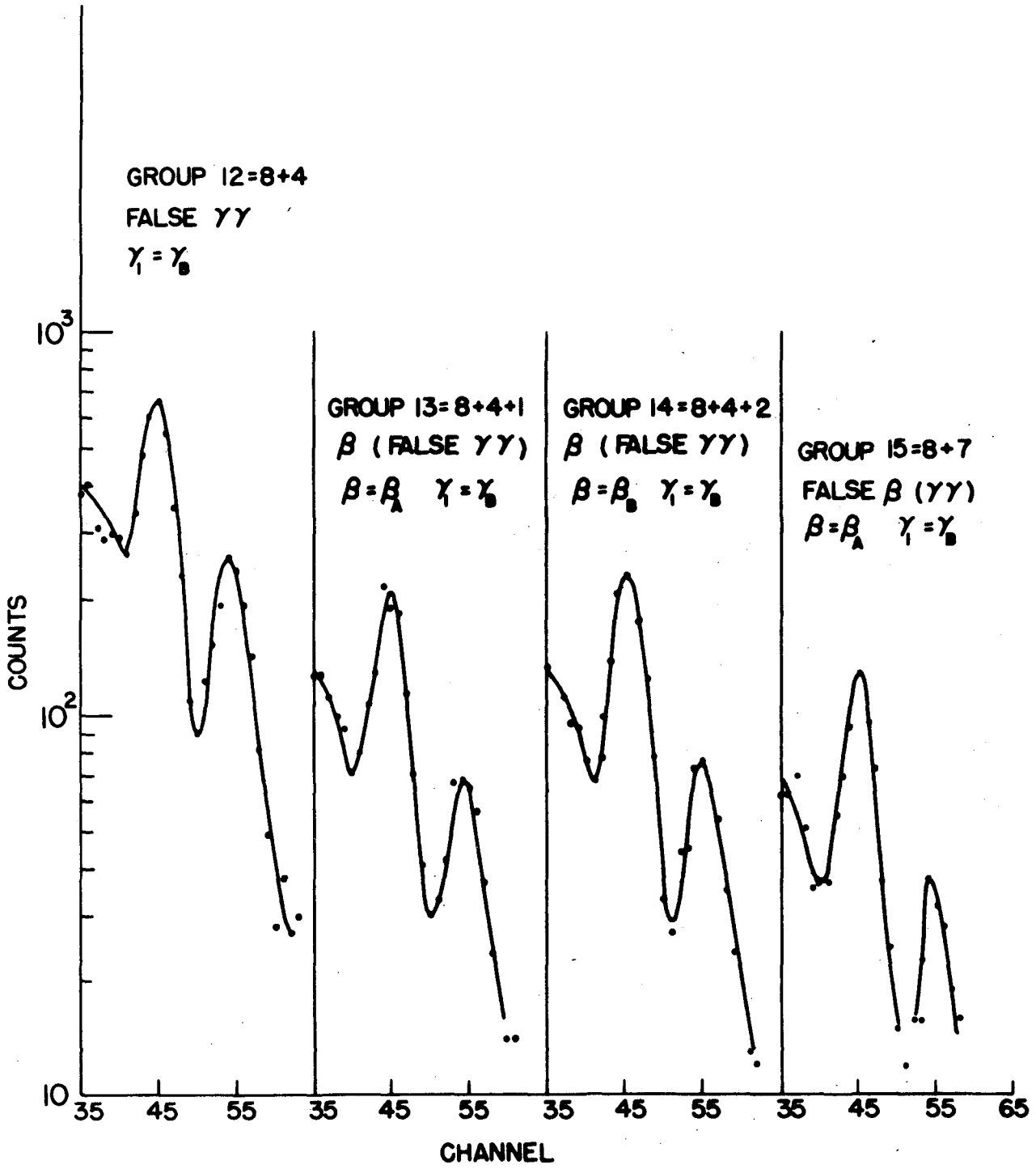
GROUP 12=8+4
FALSE γγ
γ1 = γB
GROUP 13=8+4+1
β (FALSE γγ)
β=βA γ1=γB
GROUP 14=8+4+2
β (FALSE γγ)
β=βB γ1=γB
GROUP 15=8+7
FALSE β (γγ)
β=βA γ1=γB
COUNTS
10³
10²
10
35
45
55
65
CHANNEL

We denote by FFF those accidental events in which all particles come from different nuclei. Because FFF's are counted twice in each (false $\gamma\gamma$) β group and once in each $\beta(\gamma\gamma)$ group and once in each $(\gamma\gamma)$ false β group, we add 2 X FFF in the expressions above. According to measurements and calculations, the numbers of FFF coincidences of various types can be calculated for each run by using the stored data. For example

$$F_{\gamma_{1A}} F_{\gamma_{2B}} F_{\beta_A} = \frac{(④ + ⑤ + ⑥) \times ⑦}{⓪ + ① + ② + ③ + ⑦ - (④ + ⑤ + ⑥)} \cdot \mathcal{F}(t) \quad . \qquad \text{(A22)}$$

$\mathcal{F}(t)$ is a slowly varying function of time whose value at the beginning of each run (t = 0) is 1.0 and whose value at $t = \infty$ is $\simeq 1.33$. Since the number of FFF's was less than 0.01% of the TTT's for most runs, we used $\mathcal{F} = 1.0$ in correcting the data. Because the FFF's were the same fractions of TTT's, errors in $\tilde{\epsilon}$ due to approximations in FFF's were negligible.

2. Separation of 1.81 and 2.12 MeV Photopeaks.

Nine channels (310 keV) on either side of the valley between the photopeaks were chosen for data analysis. Peaks and valleys were taken from inspection of groups ⓪ and ⑧ . We compared the Mn^{56} gamma spectra with superimposed Ce^{144} and Y^{88} spectra (with prominent 2.18 and 1.84 MeV transitions) and obtained the following prescriptions for separating the Mn^{56} photopeaks:

$$(\overline{TTT})_{1.81} = \left((TTT)^{peak}_{1.81} - f_1 \cdot (TTT)^{peak}_{2.12}\right) / (1 - f_1 f_2)$$
$$(\overline{TTT})_{2.12} = \left((TTT)^{peak}_{2.12} - f_2 \cdot (TTT)^{peak}_{1.81}\right) / (1 - f_1 f_2) \qquad \text{(A23)}$$

For the first half of the analyzer $f_1 = 0.873$, $f_2 = 0.129$.

For the second half $f_1 = 0.751$, $f_2 = 0.126$.

3. Calculation of $\tilde{\epsilon}$ and $\delta\tilde{\epsilon}_{st}$ from Data.

We found u and $\tilde{\epsilon}$ for each run according to the equations of Chapter II. (Eqns. (9) and (10))

$$U = \left(\overline{T_{\gamma_{1A}} T_{\gamma_{2B}} T_{\beta_A}} \Big/ \overline{T_{\gamma_{2B}} T_{\gamma_{1B}} T_{\beta_A}}\right) \cdot \left(\overline{T_{\gamma_{1B}} T_{\gamma_{2A}} T_{\beta_B}} \Big/ \overline{T_{\gamma_{1A}} T_{\gamma_{2B}} T_{\beta_B}}\right)$$

$$\epsilon = \tfrac{1}{2}(U-1)/(U+1) \qquad \text{(A24)}$$

The statistical error in $\tilde{\epsilon}$, denoted $\delta\tilde{\epsilon}_{st}$ is given by

$$\delta\tilde{\epsilon}_{st} = \frac{1}{4}\left(\sum_{i=1}^{4} (\delta U_i)^2\right)^{1/2} . \qquad \text{(A25)}$$

The δU_i are the fractional errors in each of the four TTT's.

For example

$$\delta U_{\left(T_{\gamma_{1A}} T_{\gamma_{2B}} T_{\beta_A}\right)_{1.81}} = \frac{\left[\left(① + ⑤ + ⑦\right)_{1.81} + f_1^{\,2}\left(① + ⑤ + ⑦\right)_{2.12}\right]^{1/2}}{1 - f_1 f_2} . \qquad \text{(A26)}$$

4. Normalization Using $\gamma\gamma$ Coincidences.

For the case in which double coincidences are used for normalization (Eqns. (13) - (16))

$$U_A = \left(\overline{T_{\gamma_{1A}} T_{\gamma_{2B}} T_{\beta_A}} \Big/ \overline{T_{\gamma_{1A}} T_{\gamma_{2B}}}\right) \cdot \left(\overline{T_{\gamma_{2A}} T_{\gamma_{1B}}} \Big/ \overline{T_{\gamma_{2A}} T_{\gamma_{1B}} T_{\beta_A}}\right)$$

$$U_B = \left(\overline{T_{\gamma_{1B}} T_{\gamma_{2A}} T_{\beta_B}} \Big/ \overline{T_{\gamma_{1B}} T_{\gamma_{2A}}}\right) \cdot \left(\overline{T_{\gamma_{2B}} T_{\gamma_{1A}}} \Big/ \overline{T_{\gamma_{2B}} T_{\gamma_{1A}} T_{\beta_B}}\right) \qquad \text{(A27)}$$

$$\tilde{\epsilon}_{A(B)} = (U_{A(B)} - 1)/(U_{A(B)} + 1)$$

Photopeak separation takes the same form as (A23). Error analysis is complicated by $\gamma\gamma$'s. Since some groups enter both doubles and triples expressions, careful attention must be paid to the analysis. Statistical errors $\delta\tilde{\epsilon}_{A_{st}}$ and $\delta\tilde{\epsilon}_{B_{st}}$ are seen to be square roots of sums of thirty-two terms.

BIBLIOGRAPHY

1. J. H. Christenson, J. W. Cronin, V. L. Fitch, and R. Turlay, Phys. Rev. Letters 13, 138 (1964).
2. J. Bernstein, G. Feinberg, and T. D. Lee, Phys. Rev. 139, B1650 (1965).
3. S. P. Lloyd, Phys. Rev. 81, 161 (1951).
4. T. D. Lee and C. N. Yang, Brookhaven National Laboratory Report BNL - 443, 1957 (unpublished)
5. E. M. Henley and B. A. Jacobsohn, Phys. Rev. 113, 225 (1959); E. M. Henley and B. A. Jacobsohn, Phys. Rev. 113, 234 (1959).
6. P. Stichel, Z. Physik, 150, 264 (1958).
7. V. DeSabbata, Nuovo Cimento 21, 659 (1961); V. DeSabbata, Nuovo Cimento 21, 1058 (1961).
8. E. Fuschini, V. Gadjokov, C. Maroni, and P. Veronesi, Nuovo Cimento 33, 709, (1964); E. Fuschini, V. Gadjokov, C. Maroni, and P. Veronesi, Nuovo Cimento 33, 1309 (1964).
9. P. Dagley, M. A. Grace, J. Gregory, and J. Hill, Proc. Roy. Soc. (London) 250, 550 (1959).
10. F. R. Metzger and W. B. Todd, Phys. Rev. 92, 904 (1953).
11. N. Levine, H. Frauenfelder, and A. Rossi, Z. Physik 151, 241 (1958).
12. L. Rosenfeld, Oriented Nuclei (Copenhagen, 1959).
13. E. M. Henley and B. A. Jacobsohn, Phys. Rev. Letters 16, 706 (1966).

VITA

Martin Henry Garell [redacted]

[redacted] entered Princeton University and received his Bachelor or Arts degree in Physics in 1960. While attending Princeton, he wrote his Bachelor's thesis under Professor R. Sherr. He enrolled at the University of Illinois as a graduate student in the fall of 1960, having received a National Science Foundation Cooperative Fellowship for that year. During his stay at Illinois, he served as a teaching assistant in undergraduate physics courses for two years and as a research assistant for five years. He received his Master of Sciences degree in 1962 and is a member of the American Physical Society.